THE UNIVERSITY OF ADELAIDE
AUSTRALIA

Structural and geochronological constraints on the origin and evolution of rocks in the Ormiston Pound region of the Western MacDonnell Ranges, Northern Territory

David Haddow

Tectonics, Resources and Exploration
Department of Geology and Geophysics
School of Earth and Environmental Sciences
University of Adelaide, South Australia
david.haddow@student.adelaide.edu.au

26 October 2009

Table of Contents

Structural and geochronological constraints on the origin and evolution of rocks in the Ormiston Pound region of the Western MacDonnell Ranges, Northern Territory

David Haddow, University of Adelaide

Abstract

The Arunta Inlier preserves a complex structural history, subject to a series of igneous, metamorphic and deformational events from the Paleoproterozoic to the mid-Paleozoic. U-Pb detrital zircon ages from Paleoproterozoic and Neoproterozoic sediments at Ormiston Gorge coincide with the timing of various tectonic phases in the Arunta Inlier. First order interpretations suggest that the Northern Arunta Inlier was the source of the oldest zircons recorded at ~1820 Ma, coinciding with the timing of the Stafford Event. The Strangways Orogeny at ~1770 Ma and 1730 Ma is the earliest deformation preserved in the Central Arunta Inlier and is probably the source of zircons accumulated in these sediments. Zircons post-dating the Strangways Orogeny are likely sourced from the Southern Arunta Inlier, coinciding with the Argilke Tectonic Event at ~1680 Ma, the Chewings Orogeny at ~1600 Ma, the Anmatjira Uplift Phase at 1500-1400 Ma and the emplacement of the Teapot Granite Complex at ~1140 Ma. The Neoproterozoic Heavitree Range Quartzite sediments represent initial deposition in the Amadeus Basin, which forms the remnant of a once much larger intracratonic basin in central Australia known as the Centralian Superbasin. The Arunta Inlier was exhumed from beneath the Centralian Superbasin during the Devonian-Carboniferous Alice Springs Orogeny, forming a series of sub-basins including the Amadeus, Ngalia and Georgina Basins. North-south crustal compression during this Orogeny reactivated a series of steep north-dipping Mesoproterozoic fault structures including the Redbank shear zone and the Ormiston thrust zone. The northern Amadeus Basin is characterised by coupled basement and cover deformation, producing a series of basement-rooted south-propagating thrusts, which penetrate the basal Heavitree Range Quartzite. Structural cross-sections constructed across the Ormiston region propose a series of splay thrusts within the Ormiston thrust zone, with the basement and Heavitree Quartzite heavily deformed. The conformably overlying Bittersprings Formation comprises salts and evaporates,

interpreted as a detachment layer. $^{40}Ar/^{39}Ar$ muscovite dating of mylonitic shear zones at Ormiston Gorge have constrained 'peak deformation' conditions in the region to a minimum age of 350 ± 3 Ma. Mineral assemblages formed in the surrounding areas reflect greenschist to lower amphibolite facies metamorphism, with temperatures reaching at least 350°C.

Key words: Alice Springs Orogeny, Amadeus Basin, Heavitree Quartzite, Neoproterozoic, Arunta Inlier, Redbank shear zone, Ormiston thrust zone, peak deformation.

1. Introduction

A series of igneous, metamorphic and deformational events have occurred in the Arunta Inlier spanning the Paleoproterozoic to the mid-Paleozoic (Black & Shaw, 1992a). Exhumed during the Devonian-Carboniferous Alice Springs Orogeny (Flottmann & Hand, 1999), the Arunta Inlier (Figure 1) comprises low to high-grade mineral assemblages ranging from greenschist to granulite facies (Warren & Shaw, 1995). Exhumation of granulite facies rocks has produced a high gravity anomaly to the north of the Redbank Shear Zone and along the Strangways Metamorphic Complex (Anfiloff & Shaw, 1973; Teyssier, 1985).

Further south, the Amadeus Basin contains Neoproterozoic sediments that overlie and define the southern margin of the Arunta Inlier. Coupled basement and cover deformation caused by the Alice Springs Orogeny is well preserved along the northern margin of the Amadeus Basin, particularly at Ormiston Gorge where thrust faulting is evident within the Heavitree Range Quartzite.

This study uses $^{40}Ar/^{39}Ar$ dating of mylonitic shear zones from Ormiston Gorge to better constrain the timing of deformation along the northern margin of the Amadeus Basin. Previous studies focussing on the timing of the Alice Springs Orogeny include $^{40}Ar/^{39}Ar$, K/Ar, Rb/Sr and apatite fission track dating, revealing that this Orogeny occurred over the interval 450-300 Ma (Shaw & Black, 1991; Shaw et al., 1992).

The Heavitree Range Quartzite is the basal unit of the Amadeus Basin sedimentary succession. Initial deposition along the northern margin of the Amadeus Basin is constrained in this study by Laser Inductively Coupled Plasma Mass Spectrometry (LA-ICPMS) U-Pb dating of detrital zircons within the basal pebble deposits of the Lower Heavitree Quartzite. The age of the Chewings Range Quartzite occupying the eastern ridge of the Ormiston Pound is also constrained in order to compare with previous deposition age estimates (Marjoribanks & Black, 1974). These zircon ages will be further used to provide a first order interpretation in regards to the origin of each zircon by comparing the age with the timing of events in the Arunta Inlier (Table 1)

Provided that the timing of deposition and deformation in this region are constrained, the validity of surface geology maps and cross sections can be examined.

ArcGIS and 2D Move software are used in this study to produce structural cross-section across Ormiston Gorge, following on from the work of Flottmann and Hand (1999) whom provided restored cross-sections across the Ormiston Gorge and Mount Sonder regions. The cross-sections express the structural deformation generated by the Alice Springs Orogeny, with the formation of nappe-style fold structures in the transitional zone between the Arunta basement province and the north margin of the Amadeus Basin. Southward verging duplex structures penetrating into the Heavitree Range Quartzite are evident (Flottmann & Hand, 1999) and are the source of the mylonitic shear zones dated in this study.

2. Geological Setting

Central Australia has been the focus of two major intracontinental deformation events since the Late Proterozoic, both related to crustal-scale north-south shortening in the region. The Musgrave Province was exhumed from depths of 40-45 km during the Neoproterozoic to Early Cambrian (600-565 Ma; Wade et al., 2005; Raimondo et al., 2009) Petermann Orogeny. The exhumed basement rocks of the Musgrave Province fragmented the previously continuous Centralian Superbasin, forming the Officer Basin to the south of the region. The Mid- to Late Paleozoic (450-300 Ma; Haines et al., 2001) Alice Springs Orogeny was onset by the reactivation of the northward dipping Redbank Thrust Fault in the Arunta Inlier, preferentially orientated for reactivation during north-south crustal-compression. The Arunta Inlier was exhumed from beneath the remnant Centralian Superbasin during this Orogeny, forming a series of sub-basins including the Amadeus, Ngalia and Georgina Basins (Lindsay & Korsch, 1991).

The crustal-scale Redbank Shear Zone illustrated in Figure 1 was the principle fault system active during the Alice Springs Orogeny with faults dipping north at >45° into the lower crust and mantle (Flottmann & Hand, 1999). This highly deformed zone comprises a steeply north-dipping schistose mylonitic foliation fabric and an extension lineation that plunges down dip (Obee & White, 1985). The fault zone offsets the Moho by >10 km (Flottmann & Hand, 1999) and is thought to have

reactivated north-dipping Mesoproterozoic thrust faults in the surrounding area including the Ormiston thrust.

Nappe-style fold structures developed in the transitional zone between the exhumed Arunta Inlier and the Amadeus Basin were associated with moderate shortening. Seismic data suggested that the basement fault zones (e.g. Redbank shear zone and the Ormiston Thrust) dipped north at 35-45°. $^{40}Ar/^{39}Ar$ data obtained from biotite and K-feldspar studies (Shaw et al., 1992) suggest that the basement was exhumed from ≤12 km during the Alice Springs Orogeny (Flottmann & Hand, 1999).

To the south of the transition zone, the Amadeus Basin (Figure 1) is characterised by thin-skinned tectonic style shortening. This deformation was generated by basement detachment in the northern Amadeus Basin and resulted in the formation of the MacDonnell homocline. The homocline consists of steep southerly and (overturned) northerly dips of the entire sedimentary succession, striking east-west across >200 km (Flottmann & Hand, 1999).

3. Stratigraphy of the Ormiston region

The southern Arunta Inlier comprises a series of igneous and metamorphic rock packages formed during the Paleoproterozoic (Table 1). Basement rocks of the Arunta Inlier and the ~1060 Ma Stuart Dykes (Black et al., 1983; Black and Shaw, 1992a; Zhao et al., 1992; Collins and Shaw, 1995; Dunlap and Teyssier, 1995) are overlain by Neoproterozoic sediments of the Heavitree Range Quartzite and the Bitthersprings Formation in the Ormiston Gorge region (Figures 2-4; Korsch & Lindsay, 1989; Flottmann & Hand, 1999). The Amadeus Basin Upper Succession is absent from section along the northern margin of the Amadeus Basin due to uplift and erosion processes and therefore details related to the Cambrian-Devonian sediments have not been outlined in the following stratigraphy (refer to Gillam, 2005). The 'upper succession' in this study refers to sediments accumulated from the base of the Cambrian Areyonga Formation to the top of the Devonian Mereenie Sandstone.

3.1 Paleoproterozoic

3.1.1 Glen Helen Metamorphics

The Glen Helen Metamorphics (blue in Figures 1-4) comprise migmatitic quartzofeldspathic gneiss, with minor calc-silicate and quartzites outcropping to the southwest of Speares Bore (Warren and Shaw, 1995). Gneiss megacrysts evident in some areas suggest that this unit may in fact represent the granite protolith (Collins et al., 1995). Zircon core ages for the Glen Helen Metamorphics give 1680-1660 Ma and 1730 Ma (Black and Shaw, 1992a). These zircon ages coincide with the timing of the Argilke Tectonic Event in the Southern Arunta Inlier and the Strangways Orogeny in the Central Arunta Inlier respectively (Warren and Shaw, 1995). Metamorphosed under upper amphibolite facies conditions, the Glen Helen Metamorphics experienced widespread retrogression through hydration, producing biotite (Warren & Shaw, 1995).

3.1.2 Lovely Hill Schist

The Lovely Hill Schist (pink unit in Figures 1-4) outcrops along the southern margin of the Arunta Inlier (Figure 1), consisting of interlayered metamorphosed pelitic sediments and quartzofeldspathic gneiss. Minor quartz, metaconglomerate and calc-silicate rocks are also evident, with metamorphism generally occurring under lower amphibolite facies conditions. To the north of the Ormiston Thrust Zone, the schist interfingers with or unconformably overlies the Glen Helen Metamorphics (Warren & Shaw, 1995).

3.1.3 Ormiston Pound Granite

The Ormiston Pound Granite was emplaced during the Chewings Orogeny (Collins et al., 1995) and forms the basement rocks (light blue in Figures 2-4) upon which the Heavitree Range Quartzite was deposited. Dated at 1603 ± 10 Ma (Shaw et al., 1992; Collins et al., 1995), the Ormiston Pound Granite comprises north-trending dykes, gneissic granite, leucogranite and pegmatite (McLaughlin, 1994). The granite intrudes foliated granite gneisses of the Glen Helen Metamorphics and

quartzofeldspathic schist and hornblende schist of the Ryans Gap Metamorphics (Warren and Shaw, 1995). Field observations reveal a strong to weak recrystallisation and foliation of this granite, with Rb-Sr mica ages and $^{40}Ar/^{39}Ar$ mineral ages recorded at 1000 to 1100 Ma (Warren & Shaw, 1995). This age represents the timing of recrystallisation of the granite, with metamorphism occurring under amphibolite facies conditions.

3.1.4 Chewings Range Quartzite

The Chewings Range Quartzite is the north-south striking quartz ridge, which occupies the eastern margin of the Ormiston Pound (light green in Figures 1-4). The ridge comprises quartz sandstone interlayered with muscovite schist (Warren and Shaw, 1995) observed at 278031; 7384612 (UTM Zone 53S). This is indicative of greenschist to lower amphibolite metamorphic facies conditions.

Marjoribanks and Black (1974) recalculated an Rb-Sr age for a 'Potrock gneiss' located north of Mount Giles to 1587 ± 70 Ma, which has been interpreted as the maximum deformation age of the Chewings Range Quartzite. This gneiss has a siliceous composition, representing a metavolcanic unit of the Lovely Hill Schist. Deformation has been preserved in the bands of muscovite schist, with tight folding evident. A prominent east-dipping foliation is associated with the quartzite ridge, with thrust faulting responsible for repeated formations (Warren & Shaw, 1995).

3.2 Mesoproterozoic

Teapot Granite Complex

The Teapot Granite Complex is the main outcrop that occupies the area between Mount Razorback and Mount Zeil. Further south, the granite defines the northern margin of the Amadeus Basin across the Mount Sonder section (maroon in Figure 1). It consists of quartzofeldspathic gneiss, intensely migmatitic in the western outcrops. The gneiss here consists of bands less deformed than the adjacent Glen Helen Metamorphics (Warren & Shaw, 1995). The Teapot Granite cross-cuts folded Glen Helen Metamorphics to the south of the Glen Helen homestead and was dated at ~1140 Ma (Black and Shaw, 1992a).

3.3 Late Proterozoic (Neoproterozoic)

Late Proterozoic deposition within the Amadeus Basin (formerly the Centralian Superbasin) extends from the base of the Heavitree Quartzite (light orange in Figures 1-4) to the top of the Julie Formation. This succession has an average thickness of approximately 2000 m, however thickens to 4000 m in the south and 3000 m in the northeast of the basin (Gillam, 2005).

3.2.1 Heavitree Range Quartzite

The Heavitree Range Quartzite (Figure 5a and 5b) is the basal unit of the Amadeus Basin sedimentary succession (Lindsay and Korsch, 1991), distributed as a sheet across all of the major central Australian intracratonic basins (Lindsay, 1999). Massive beds of quartzite dominate the lower portion of the deposit (Figure 5c), formed by the rapid accumulation of sediment in a shallow marine environment. Initially well-sorted sandstone, these beds were lithified during a post-rift, thermal phase and are now preserved as quartzite (Gillam, 2005). This part of the unit is referred to as the Lower Heavitree Quartzite, deformed by thrust faulting and folding associated with the Alice Springs Orogeny. Mount Ormiston (Figure 5b) reveals

thrust faulting of the Lower Heavitree Quartzite, thrust on top of the younger Upper Heavitree Quartzite at 267767; 7385169 (UTM Zone 53S).

The upper portion of the formation reveals sea level fluctuation in the region, comprising inter-bedded quartzose sandstones and siltstones. Lindsay (1999) suggested at least 4 depositional sequences took place in the formation of the Upper Heavitree Quartzite. Tidal flats to high-energy shallow marine systems existed in the early stages of deposition, forming siltstones and sands respectively. The silt content of this unit allows it to behave in a relatively ductile manner, evident from the east-west striking anticline-syncline pairs developed in the region (Flottmann & Hand, 1999). Eustatic sea-level fall moved the Lower Heavitree Quartzite beds basinward and forced reworking of previously deposited sediments. Late stage shallow marine deposition followed (Gillam, 2005), continuing into the conformably overlying Bittersprings Formation.

3.2.2 Bittersprings Formation

The Bittersprings Formation (BSF) consists of the Gillen and Loves Creek Members (yellow in Figures 1-4). The Gillen Creek Member is composed of evaporates and carbonates including dolostones, limestones and siltstones. These sediments were deposited across the Amadeus Basin in a low energy, shallow marine setting at an average thickness of ~800 m (Lindsay and Korsch, 1991). Deformation of the Gillen Creek Member is evident at Ellery Creek, with disharmonic folding formed in response to compression during the Alice Springs Orogeny (Gillam, 2005; Flottmann & Hand, 1999).

The upper portion of the Loves Creek Member comprises dolostones, limestones, red calcareous siltstones and minor chert, while the lower portion consists of stromatolite biostromes. Deposition of this member was associated with a low energy lacustrine system in order to generate mixed siliciclastic and carbonate sequences (Gillam, 2005).

4. Structural setting and field relationships

North-south compression during the Alice Springs Orogeny formed southward-verging thrust faults within the Lower Heavitree Quartzite (Flottmann & Hand, 1999). This caused brittle failure of the Lower Heavitree Quartzite beds, in turn producing fault propagation thrusts along the bedding planes of the quartzite. This is evident from Mount Ormiston where Lower Heavitree Quartzite beds overlie the Upper Heavitree Quartzite. Small-scale duplex structures shown in Figure 5d illustrate a series of southward-verging horse structure revealed in Ormiston Gorge. Intense folding within the Ormiston Pound Granite (Figure 5e) is observed further east in Ormiston Pound, developing overturned folds that consist of a northward dipping axial plane (Figure 6). Kinematic indicators (Figure 5f) suggest top to the south movement, supported by lineation data expressed in Figure 7.

Thrust faulting at Ormiston Gorge caused widespread deformation across Ormiston Gorge, producing an intense east-west foliation and bedding trend across the region expressed in Figures 8 and 9 respectively. Westward plunging fold hinges (Figure 10) were evident in the western area of Ormiston Gorge, however the bedding data obtained for the Bittersprings Formation (Figure 9d) should be cautioned, due to the disharmonic nature of these evaporate beds. Studies including Marjoribanks (1976) and Flottmann and Hand (1999) suggest that this unit acted as a detachment surface during the Alice Springs Orogeny, with the Arunta basement-rooted thrusts constrained to the top of the Heavitree Quartzite. These thrusts do not pierce the upper succession along transects across the Ormiston region. However to the south and west of this area, the upper succession is pierced by north-verging backthrusts including the Gardiner Range Thrust (Flottmann & Hand, 1999).

The contact between the Heavitree Range Quartzite - Ormiston Pound Granite is unconformable along the northern Heavitree Range of Ormiston Pound. Thrusts are evident within the Lower Heavitree Quartzite beds with the Upper Heavitree Quartzite and Bittersprings Formation located in the footwall of this fault system (Warren & Shaw, 1995). Overturned anticline-syncline pairs are evident in this region and will be the focus of structural cross-sections constructed in this study.

Further east, the Chewings Range Quartzite has a strong north-south foliation trend. Thrust faulting and tight folding have been developed along this quartzite ridge, well

preserved in the interlayered bands of muscovite schist. The northern section of the ridge is partially overlain by an isolated unit of Heavitree Quartzite (Warren & Shaw, 1995). The unconformably overlying Lower and Upper Heavitree Quartzites occupy the northern area of the deposit, while the southern margin consists of quartz clasts of 1-2 cm (in diameter) within a well-foliated sand matrix. An east-west trending overturned syncline is associated with this unit, interpreted from field measurements (Figure 9e) in agreement with Warren and Shaw (1995).

5. LA-ICPMS U-Pb geochronology

The primary aim of U-Pb dating of detrital zircons was to constrain the depositional age of the Chewings and Heavitree Range Quartzites. The detrital zircons within these sediments have been sourced from a variety of different provinces within the Arunta block, which is investigated in this study.

5.1 Sample preparation

Zircon extraction was conducted at the University of Adelaide, with each quartzite sample initially crushed using a jaw crusher. The crushed sample was milled using a steel mill, with trace element contamination unimportant for zircon separation methods. Sieving of the sample was then performed using 425 μm and 75 μm mesh, separating the sample into three fractional grain sizes. Further processing of the 425–75 μm sample fraction was conducted using water and detergent, hand panning the sample to remove low-density minerals, commonly quartz in these samples. However panning the sample was not sufficient in isolating the heavier mineral components of the sample and therefore heavy liquid separation techniques were applied. The panned sample was run through a solution of methylene iodide, with magnetite and zircon fragments accumulated at the base of a separating funnel. A hand magnet was then used to remove magnetite from the refined sample, with zircon grains hand picked and mounted in epoxy resin. A separate mount was constructed for each sample, using 800 and 2400 grit to create a section through half the diameter of the

zircon grains. The zircon mount was then polished with a cloth lap before being carbon-coated at Adelaide Microscopy.

The Philips XL20 Scanning Electron Microscope and the attached Gatan CL detector were used to generate images of the zircons within each mount. The internal structure of the zircon grains was revealed by cathodoluminescence (CL) and backscattered electron (BSE) imaging techniques, using an operating voltage of 20 kV.

5.2 LA-ICPMS operating procedures and data analysis

The U-Th-Pb isotopic ratios associated with each zircon were measured using an Agilent 7500cs ICPMS at Adelaide Microscopy. A New Wave 213 nm Nd-YAG laser was used, performing the analyses using a beam diameter of 30 μm, a repetition rate of 5 Hz and a laser intensity of 70 %. Each zircon analysis was associated with an acquisition time of 100 seconds, comprising 30 seconds of background measurement, 10 seconds of beam and crystal stabilisation and 60 seconds of sample ablation, ablated in a helium atmosphere.

U-Pb fractionation was corrected by incorporating the GEMOC GJ-1 standard (Jackson et al., 2004), monitoring accuracy by repeated measurement of the Sri Lankan in-house internal standard BJWP-1. These standard samples were analysed at equal intervals in the dataset to ensure that each zircon age was associated with the same number of standard samples.

GLITTER software (Van Achterbergh et al., 2001) was used to review and refine the signal produced by the zircons and standards analysed. The refined dataset was exported and analysed using Excel macros, rearranging the dataset to evaluate the concordance associated with each zircon. Zircons associated with a concordance value of 100 ± 10 % were accepted, plotted on a Concordia curve generated using Isoplot/Ex 3.00. The error associated with individual analyses is quoted at the 1σ level.

5.3 Sample descriptions

5.3.1 Sample 40A_PQ

The Pebble Quartzite represents the basal unit of the Lower Heavitree Quartzite, comprising rounded quartz grains 0.2 ± 0.05 cm, set in a fine-grained, recrystallised quartzose matrix. Probably formed during an initial sea level transgression (Gillam, 2005), this sample was collected from Mount Ormiston at 267767; 7385169 (UTM Zone 53S), overlying the Lower Heavitree Quartzite beds. The Pebble Quartzite has been thrust over the younger stratigraphy, observed in three outcrops across the Heavitree Range. However, mapping this unit was not feasible given the large-scale on which the field map was constructed.

5.3.2 Sample 40C_LHTQ

The Lower Heavitree Quartzite consists of well-sorted sand, transported and reworked in a shallow marine setting. The shallow marine environment was developed during a period of transgression (Gillam, 2005), which initially formed the Pebble Quartzite. The Lower Heavitree Quartzite sample was collected from Ormiston Gorge at 268216; 7385116 (UTM Zone 53S), near the thrust fault contact with the underlying Bittersprings Formation (refer to Figures 2-4).

5.3.3 Sample 34B_CQ

The Chewings Range Quartzite sampled at 278031; 7384612 was taken from the southeastern region of Ormiston Pound. This unit is characterised by massive metamorphosed quartz sandstone, which is interlayered with muscovite schist. The sample is also the subject of X-ray Diffraction studies presented in this paper, due to the accessory muscovite developed in this rock during greenschist to lower amphibolite facies conditions.

5.4 Results

5.4.1 Sample 40A_PQ: zircon U-Pb dating (refer to Table 2 and Figure 11)

The majority of the zircons are elongate and rounded, with minimal prismatic shaped grains present. Little to no internal structure is evident in some of these zircons, while others express zoning, cores and/or rims (Figure 11a). Interaction between cores and rims was avoided whenever possible, however the small zircon grain size made this difficult in some instances.

The zircon ages plotted for the Pebble Quartzite in Figures 11b-d are concordant (100 ± 10%), expressing the largest population of age data at 1600 ± 10 Ma. This population represents the age of zircon cores and some rims identified from the SEM images taken prior to LA-ICPMS analysis.

Zircon ages pre-dating the cluster of data at 1600 ± 10 Ma were recorded at 1824 ± 22, 1728 ± 21 and 1676 ± 24 Ma for spots 26, 54 and 47 respectively (Figures 11b and 11c). Spots 26 and 47 represent the analysis of zircon cores, however spot 54 expressed no internal structure and therefore caution must be taken when considering this age.

Zircons ages were accumulated at ~1500-1560 Ma, producing a peak in the probability density plot illustrated in Figure 11a. These ages have been differentiated to produce separate Concordia plots for zircon cores and rims (Figure 11c and 11d respectively), with structureless grains and growth zoning evident in some of the zircons analysed.

No internal structure was identified for spots 14, 63 and 66, recording zircon ages of 1400 ± 10 Ma. These ages should be treated cautiously as the analysed area of the zircon is unclear. However spots 5, 32, 33, and 42 obtained similar ages, reflecting zircon core ages.

The youngest population of zircon ages was recorded at ~1160 ± 10 Ma, representing an accumulation of zircon rims, growth zones and structureless grains. The zircon rim data accumulated at 1160 ± 10 Ma, has generated a peak in the probability density plot of the rim data illustrated in Figure 11c.

5.4.2 Sample 40C_LHTQ: zircon U-Pb dating (refer to Table 3 and Figure 12)

The detrital zircons within the overlying Lower Heavitree Quartzite have been extensively reworked, with relatively rare core and rim sightings in this sample. Fractions of the initial zircon remain intact, with growth zoning and structureless grains dominating the sample (Figure 12a).

Zircon core ages are again concentrated at ~1600 Ma, supported by a peak in the probability density plot shown in Figures 12b and 12c. Similar to the Pebble Quartzite, some zircons pre-date these grains with an accumulation of age data at ~1690 ± 10 Ma and again at 1750 ± 10 Ma. Spots 22, 40, 44 and 59 are still unaccounted for representing growth zoning of zircons that pre-dates all other zircons recorded in the dataset. These grains represent only a fraction of the initial zircon and therefore must not be loosely interpreted.

Spots 41 and 47 represent growth zoning and a zircon core respectively, obtaining ages of ~1380 Ma. A peak in the probability density plot at ~1230 Ma represents an accumulation of zircon rims at 1200-1250 Ma. This peak is more prominent in the Concordia plot constructed for zircon rim ages shown in Figure 12d.

5.4.3 Sample 34B_CQ: zircon U-Pb dating (refer to Table 4 and Figure 13)

Prismatic shaped zircon grains exist in the Chewings Range Quartzite, while the terminations in other grains have been rounded. Euhedral growth zoning dominates a large portion of the age data obtained, with minor zircon cores, rims and structureless grains present (Figure 13a). Zircon core age data accumulates at 1770 ± 10 Ma, while a second population is obtained at 1730 ± 10 Ma. These ages are expressed on the Concordia diagram and probability density plot shown in Figures 13b and 13c.

An accumulation of zircon ages occurs at 1650 ± 10 Ma, with zircon core ages extending to 1578 ± 21 Ma (Figure 13c). Spots 17 and 66B obtained concordant ages for the same zircon core at 1148 ± 16 Ma and 1142 ± 17 Ma, with the repeated analysis used to confirm the age data collected from the first measurement.

5.5 Provenance interpretations of zircon ages

The tectonic evolution of central Australia is summarised in Table 1 (Collins & Shaw, 1995; Dunlap & Teyssier, 1995) and is used to interpret the source of detrital zircon accumulated along the northern margin of the Amadeus Basin.

5.5.1 Sample 40A_PQ – Pebble Quartzite

The Pebble Quartzite zircon core ages accumulated at ~1600 Ma have been directly sourced from the underlying Ormiston Pound Granite (1603 ± 10 Ma; Collins et al., 1995). Rare zircons pre-dating the emplacement of the granite coincide with periods of granulite facies conditions in the Southern and Central Provinces of the Arunta Inlier. These zircons occupy <10 % of the dataset due to the larger accumulation of zircons locally derived from the Ormiston Pound Granite.

A minor proportion of zircons post-dating the Ormiston Pound Granite emplacement were accumulated at 1440-1440 Ma (Figure 11b). These zircons were likely sourced from granulite facies mineral assemblages developed along the southern margin of the Mount Chapple massif in the Redbank Hill massif (Warren & Shaw, 1995). The Teapot Granite Complex (1140 Ma; Black and Shaw, 1992a) post-dates these zircons, coinciding with zircon rims ages collected at 1145 ± 10 Ma. These zircon rims (Figure 11d) likely represent the timing of metamorphism in the Southern Province, with extensive migmatisation and pegmatite generated during emplacement of the this granite complex (Marjoribanks and Black, 1974).

5.5.2 Sample 40C_LHTQ – Lower Heavitree Quartzite

A large cluster of zircon core ages are accumulated at ~1600 Ma for the Lower Heavitree Quartzite. This is consistent with the underlying Pebble Quartzite, however Figure 10a represents a plot of all the zircon data collected, revealing peak accumulation at ~1680 Ma. Intense migmatisation in the Glen Helen Metamorphics coincides with this peak position.

Zircons pre-dating this event are represented by cores (Figure 12c), growth zoning and some zircons expressing little internal structure. These zircons coincide with the age of felsic and mafic mineral assemblages formed in the Northern and Central Provinces of the Arunta Inlier at ~1770 Ma and ~1730 Ma (Dunlap & Teyssier, 1995). However the dataset does not comprise adequate zircon age data corresponding to these events and therefore sourcing zircons from these areas cannot be interpreted with certainty.

Zircon rims recorded at ~1500 Ma were likely sourced from the Southern Arunta Province. Amphibolite to granulite facies mineral assemblages were formed in this region between ~1500-1400 Ma (Warren & Shaw, 1995). The latter was developed in the Southern Arunta Province, with zircons forming under dry conditions. Therefore these zircons were probably sourced from the southern margin of the Mount Chapple massif, in the Redbank Hill massif and from locally metamorphosed regions (Warren & Shaw, 1995).

The youngest zircon peak in the probability density plot (Figure 12d) at ~1150 Ma reflects zircon rim data. This again coincides with the timing of emplacement of the Teapot Granite Complex in the Southern Province of the Arunta Inlier.

5.5.3 Sample 34B_CQ – Chewings Range Quartzite

The Chewings Range Quartzite has inherited 1770 ± 10 Ma and 1730 ± 10 Ma zircon cores, coinciding with the age of felsic and mafic rocks located in the Northern and Central Provinces of the Arunta Inlier (Warren & Shaw, 1995). Zircons recorded at ~1650 Ma correspond to the Southern Province, where migmatitic gneiss has been previously dated within the Glen Helen Metamorphics at ~1680 Ma (Black & Shaw, 1992a).

5.6 Constraining the timing of deposition

5.6.1 Sample 40A_PQ – Pebble Quartzite

The Pebble Quartzite beds were not metamorphosed prior to the Alice Springs Orogeny and therefore deposition of the basal sediment occurred post-Teapot Tectonomagmatic Event (~1140 Ma; Black and Shaw, 1992a). The youngest concordant zircon in the dataset was recorded at 1047 ± 13 Ma for spot 4, which coincides with the timing of emplacement of the Stuart Dykes. This represents the maximum timing of initial deposition in the Amadeus Basin.

5.6.2 Sample 40C_LHTQ – Lower Heavitree Quartzite

The youngest concordant zircon in the dataset was recorded at 1107 ± 13 Ma, representing the maximum depositional age of the Lower Heavitree Quartzite. However the maximum age constraint obtained for the underlying Pebble Quartzite further constrains the depositional age of this unit to a maximum age of 1047 ± 13 Ma.

5.6.3 Sample 34B_CQ – Chewings Range Quartzite

Deposition of the Chewings Quartzite is constrained by the youngest concordant zircon core age accepted in the dataset. Zircon rims cannot be used to constrain deposition because the Chewings Quartzite has been metamorphosed. The zircon core ages obtained at 1145 ± 5 Ma coincide with the timing of the Teapot Granite Complex (Black and Shaw, 1992a). However these ages were obtained from the same zircon core, meaning only one zircon in the dataset yielded an age of 1145 ± 5 Ma. Constraining the timing of deposition of the Chewings Range Quartzite is not adequate from this single zircon age because contamination during sample preparation could have occurred.

The Chewings Quartzite was deposited directly on top of basement rocks in the southern Arunta Inlier, which may explain the large accumulation of zircon core ages that pre-date the Chewings Orogeny. If this age were accepted, the Chewings

Quartzite would have been deposited later during the Mesoproterozoic. Deposition of the Chewings Quartzite has been interpreted in the absence of this zircon core age, generating a maximum age of 1578 ± 21 Ma.

6. $^{40}Ar/^{39}Ar$ geochronology of mylonitic shear zones

Mylonitic shear zones developed in the Heavitree Range Quartzite have been examined in this study to constrain the timing of deformation at Ormiston Gorge. Two mylonite samples collected during field studies at Ormiston Gorge in July 2008 were sampled from these thrusts within the Ormiston duplex. $^{40}Ar/^{39}Ar$ dating of muscovite was used to date these shear zones, less susceptible to contamination by uptake of excess argon in comparison to biotite for example (Harrison and Zeitler, 2005).

6.1 Sample preparation

The mylonite fault rocks were crushed using a jaw crusher, before optically transparent muscovites were separated from the mylonite sample using a Frantz magnetic separator and hand picked under a binocular microscope. The selected grains were then leached in dilute hydrofluoric acid (HF) for one minute, before being thoroughly rinsed with distilled water in an ultrasonic cleaner.

The muscovite samples were loaded into two large wells comprising a 1.9 cm diameter and 0.3 cm depth aluminium disc. The aluminium discs were shielded from cadmium in order to minimise nuclear interference reactions that may occur during irradiation of the sample. The wells were grouped by smaller wells including the Fish Canyon sanidine, monitoring neutron fluence and therefore adopting an age of 28.03 ± 0.078 Ma. The samples were then irradiated for 25 hours in a nuclear reactor at Lucas Heights, New South Wales, with mean J-values calculated from standard grains within the small pits equal to 0.0089480 ± 0.0000036 for the muscovite samples, ORM7 and ORM8. This value represents the average and standard deviation of J-values of the small wells for each irradiated disc.

Mass discrimination was monitored throughout the analysis of each muscovite sample using an automated air pipette. The mean mass discrimination value was calculated at 1.001227 ± 0.36 per Dalton (atomic mass unit) for sample ORM7 and 1.001198 ± 0.36 per Dalton for sample ORM8. The correction factors considered from the interference of isotopes in these samples were $(^{39}Ar/^{37}Ar)_{ca} = 7.30x10^{-4}$ (± 11%), $(^{36}Ar/^{37}Ar)_{ca} = 2.82x10^{-4}$ (± 1%) and $(^{40}Ar/^{39}Ar)_{k} = 6.76x10^{-4}$ (± 32%).

6.2 $^{40}Ar/^{39}Ar$ dating procedures and data analysis

Samples ORM7 and ORM8 were step-heated using a 110 W Spectron Laser System associated with an Nd-YAG (IR; 1064 nm) laser. Three SAES AP10 getters and a liquid nitrogen condensation cap were used to ensure gas purification in a stainless steel extraction line. Ar isotopes were measured using a MAP 215-50 mass spectrometer, analysed at a resolution of ~600 with a sensitivity of 2×10^{-14} mol/V. 9-10 cycles of peak hopping were associated with a Balzers SEV 217 electron multiplier, running the Argus program written by M.O. McWilliams under a LabView environment in order to obtain the required data. ArArCALC software (Koppers, 2002) was used to process and refine the raw data obtained from the analysis, calculating muscovite ages using the decay constants recommended by Steiger and Jager (1997).

Blank samples were analysed between every 3 to 4 steps in the analysis with ^{40}Ar blanks ranging from 1×10^{-16} to 2×10^{-16} mol. The argon isotopic data expressed for incremental heating of samples ORM7 and ORM8 has been corrected for blanks, mass discrimination and radioactive decay.

Plateau ages obtained using $^{40}Ar/^{39}Ar$ dating methods must include at least 70 % of ^{39}Ar, with the plateau constructed over a minimum of three consecutive steps. If these criteria are met, the plateau age can be analysed more vigorously, assessing the validity of the age using Chi Square Statistics. The Mean Square Weighted Deviate (MSWD) value calculated for the plateau and isochron age plots is the first consideration of this test. The second requirement is the number of degrees of freedom associated with the dataset; calculated by N-1 for plateau age analysis or N-2 for isochron age analysis for straight line fitting purposes, where N is the number of

steps used to obtain the age recorded. The Chi Square value, χ^2 is the final requirement of this test, calculated as the product of the MSWD value and the number of degrees of freedom.

Once these three values have been obtained, the relevant Chi Square Table can be used to evaluate the probability of occurrence (p-value) for the plateau or isochron age obtained from the dataset. If the p-value is <0.05 (95% confidence level) then the age can be rejected.

6.3 Results

6.3.1 Sample ORM7

The muscovite analysed in sample ORM7 defines a plateau age of 350 ± 3 Ma (Figure 14a). This age was obtained using 11 consecutive steps, using 95% of ^{39}Ar (Table 5). The corresponding normal isochron age is equal to 347 ± 8 Ma (Figure 14b).

6.3.2 Sample ORM8

Sample ORM8 is associated with a plateau age of 380 ± 4 Ma (Figure 15a), defined by 4 consecutive steps and 30 % ^{39}Ar (Table 6). The plateau age plot expresses a saddle-shaped age spectra, as opposed to the horizontal age plateau obtained for Sample ORM7. The corresponding normal isochron age could not be obtained (Figure 15b).

6.4 Constraining the timing of deformation

6.4.1 Sample ORM7

The muscovite analysed in sample ORM7 shows no indication of excess argon, obtaining a plateau age of 350 ± 3 Ma (Figure 14a). The sample satisfies the initial criteria required for producing a reliable plateau age and therefore Chi-statistics have been applied. 10 degrees of freedom were associated with this plateau age, with an MSWD value equal to 1.41. Therefore the $\chi 2$-value is 14.1, corresponding to a p-value of 0.1684 (i.e., 0.250 < p-value > 0.100). The probability of occurrence is >0.05 and so the plateau age is accepted. Hence 350 ± 3 Ma reflects the time at which temperatures cooled through the closure temperature of muscovite at ~350°C.

The normal isochron age supports the plateau age estimate, equal to 347 ± 8.20 Ma. This age is associated with an MSWD value of 1.29 and 9 degrees of freedom, producing a $\chi 2$-value of 11.61. This value corresponds to a p-value of 0.2361 (i.e., 0.250 < p-value >0.100), making the isochron age acceptable.

6.4.2 Sample ORM8

The age spectra for sample ORM8 (Figure 15a) shows that the muscovite crystals analysed in sample ORM8 probably contained excess argon, generating a saddle-shaped age spectra (Lanphere and Dalrymple, 1976). 30% ^{39}Ar was used to calculate a plateau age of 380 ± 4 Ma, associated with 4 consecutive steps. This age appears to plateau earlier than expected (older age) and therefore the plateau age represents the maximum crystallisation age of muscovite along this shear zone.

8. Construction of Ormiston Gorge cross-sections

8.1 Cross-section inputs

Existing geological maps (Warren & Shaw, 1995) and cross-sections (Flottmann & Hand, 1999; Gillam, 2005) were used together with field data measurements collected during fieldwork in July 2009 to generate a series of cross-sections across the Ormiston Gorge region. Midland Valley's 2D Move software was used to construct these sections, integrating the information provided by these sources. However it is important to understand that these sections are only a representation of the basement-cover interaction across this area and have not been balanced or restored.

8.1.1 Maps

The existing 1:250 000 Hermannsburg geological map sheet (Warren & Shaw, 1995) provides the basic framework for section construction. The structural geology of the region was constructed from field mapping shown in Figures 2-4, illustrating basement-cover interaction. The 1:1,000,000 surface geology map provided by Liu et al. (2006) was referred to in areas of Ormiston Gorge that were inaccessible due to the challenging terrain.

8.1.2 Cross-sections

Gillam (2005) constructed and restored five cross-sections across the Amadeus Basin, providing details of the deformation accommodated within each unit during the Alice Springs Orogeny. These sections were constructed in accordance with Flottmann and Hand (1999), considering the lower Bittersprings Formation as a detachment surface.

The Palm Valley section constructed by Gillam (2005) showed that the basement-rooted Redbank Thrust Fault Zone penetrated through the Heavitree Quartzite at the northern end of the section. This southward verging thrust system was responsible for the formation of the Razorback structure in the footwall of the MacDonnell

Homocline (Figures 16 and 17 - Flottmann & Hand, 1999; Gillam, 2005), indicating that the Redbank shear zone represents a crustal scale ramp.

Further south, the Ormiston Gorge cross-section constructed and restored in the work of Flottmann and Hand (1999) (Figures 18 and 19) was used to quantify the amount of shortening and vertical exhumation that had occurred along the northern margin of the Amadeus Basin.

8.2 Limitations of the cross-sections

Volume balancing of the Bitthersprings Formation is difficult to quantify due to the disharmonic folding that occurs in this unit. The Bitthersprings Formation was constructed at an average thickness of 2000-2500 m (Gillam, 2005), using measured field data to determine the general trend of folding within these beds (Figure 5e). Therefore the anticline-syncline pairs illustrated in section are not a true representation of the position of folds in the Bitthersprings Formation and instead only highlight the disharmonic nature of this unit.

The Ormiston Pound cross-section is poorly constrained due to poor outcrop data collected along this transect. Access to this region was difficult and thus structural work regarding this area of the Heavitree Range was interpreted from several cross-sections constructed from observation and sketches noted from the Chewings Quartzite Ridge (looking west). Thrust faulting appeared evident from the uplift of the Heavitree Range behind the Ormiston Pound, with the quartzite beds orientated at ~35°. A geological map constructed by Warren & Shaw (1995) confirmed two east-west striking faults, associated with two overturned anticlines and an overturned syncline (Figure 23).

8.3 Assumptions of the cross-sections

Although the sections have been constrained by the geological maps and restored cross-sections previously discussed, several assumptions have been made in order to construct them.

1) Basement culmination in the Ormiston region is constructed in accordance with Flottmann and Hand (1999).

2) The Heavitree Quartzite is assumed to maintain a relatively constant thickness, constructed in these sections at a thickness of ~500 m (Gillam, 2005).

3) Mylonitic shear zones found along the northern Heavitree Range are interpreted as splay faults of the Ormiston thrust.

4) The overlying Bitterspring Formation has been constructed independently from the underlying geology. The lower Bitterspring beds are interpreted as a detachment surface, assumed to deform non-elastically (Gillam, 2005).

8.4 Location and key features of the cross-sections generated in this study

8.4.1 West of Ormiston Gorge section

The cross-section west of Ormiston Gorge (Figure 20) was constructed through the western Heavitree Range Quartzite from 266364; 7393203 to 266364; 7374840 (UTM Zone 53S). The section trace intersects basement rocks of the Arunta Inlier in the north of the section, which thrust southward over the Heavitree Quartzite and Bitterspring Formation. A second thrust constructed further south defines the contact between the Lower Heavitree Quartzite and the underlying Upper Heavitree Quartzite. The Upper Heavitree Quartzite in the footwall of this thrust is well folded, with the Bitterspring Formation deposited in the southern limb of this structure.

8.4.2 Ormiston Gorge section

The Ormiston Gorge cross-section (Figure 21) was constructed through the Heavitree Range Quartzite along a north-south section east of Mount Ormiston from 268333; 7389375 to 268333; 7372489 (UTM Zone 53S). The section intersects basement rocks of the Arunta Inlier, which again thrust southward along the Ormiston Thrust over the Neoproterozoic Amadeus Basin sediments (Flottmann & Hand, 1999). South of this position, the Lower Heavitree Quartzite propagates southward with thrusts evident within the Lower Heavitree Quartzite beds and along the contact with the Bitterspring Formation further south. Folding is developed south of this contact with Heavitree Quartzite outcropping within the Bitterspring Formation cover sequence. Outcrop here represents the erosional remnants of an east-west trending anticline.

8.4.3 Back Gorge section

The Back Gorge section (Figure 22) runs southeast across the Heavitree Range Quartzite from 268480; 7388248 to 271260; 7384445 (UTM Zone 53S). The Arunta Inlier in the north of the section is uplifted along the Ormiston thrust, comprising a series of splay faults in the footwall of this thrust. Lower Heavitree Quartzite beds have been thrust over the Upper Heavitree Quartzite at the top of the Heavitree Range, while at the base of the Heavitree Range, thrust faulting was revealed by the formation of mylonites in the Back Gorge. It is important to recognise that mylonite shear zones were developed in the western mapping area of Ormiston Gorge (Figure 3), however these zones are too small to map. Hence their absence from the section.

8.4.4 Ormiston Pound section

The cross-section (Figure 23) was constructed north-south across Ormiston Pound from 274276; 7392200 to 274234; 7376202 (UTM Zone 53S). The Lower Heavitree Quartzite beds in the footwall of the Ormiston thrust dip north at ~35°, reflecting the development of south propagating fault zones in the region. Overturned anticline-syncline pairs have been interpreted within the Lower Heavitree Quartzite (Warren & Shaw, 1995). Further south the Lower Heavitree Quartzite unconformably overlies

the Ormiston Pound Granite, expressing no evidence of thrust faulting (Warren & Shaw, 1995).

The Ormiston Pound Granite - Lower Heavitree Quartzite contact along the southern margin of Ormiston Pound is defined by south-verging thrust system, which penetrates the Heavitree Range Quartzite. The Lower Heavitree Quartzite beds have been folded with splay faults constructed further south defining the contact between the Lower (hangingwall) and Upper Heavitree Quartzite (footwall).

9. Discussion

In a review of all previous geochronology studies from the southeastern Arunta Inlier (Dunlap & Teyssier, 1995), most analyses have focussed on dating Proterozoic high-grade rocks. However these rocks comprise a complex thermal and deformation history, which may produce inconsistent age data making metamorphic events difficult to interpret. The revised nomenclature of Collins and Shaw (1995) reveals the last 6 tectonic events to occur in the Arunta block and is summarised in Table 6.

The Northern and Central Provinces of the Arunta Inlier developed granulite facies mineral assemblages during the Stafford Event at ~1820 Ma and the Strangways Orogeny at ~1770 Ma and ~1730 Ma (Black and Shaw, 1992a). U-Pb detrital zircon ages coinciding with this event are largely accumulated in the Paleoproterozoic Chewings Range Quartzite, however only comprise ~5% of the age data collected for the Neoproterozoic Heavitree Range Quartzite. The latter sediments directly overly the Ormiston Pound Granite (~1600 Ma; Collins et al., 1995) readily accumulating zircons from this locally derived source. In comparison, the Chewings Range Quartzite is underlain by basement rocks of the Arunta Inlier, which pre-date the timing of emplacement of the Ormiston Pound Granite. Therefore zircons accumulated in the Chewings Range Quartzite have been sourced from the Arunta Inlier in provinces formed before 1600 Ma.

Zircons accumulated at 1650 ± 10 Ma in the Chewings and Heavitree Range Quartzites were likely derived during the Argilke Tectonic Event, active in the Southern Arunta Inlier. The Glen Helen Metamorphics reflect these zircon ages, where a north-south foliation trend was developed (Warren & Shaw, 1995). This was

caused by intense migmatisation in the region, with maximum deformation interpreted at ~1680 Ma for zircons dated in migmatitic gneiss southwest of the Glen Helen homestead (Black and Shaw, 1992a). Collins et al. (1995) dated zircon cores and rims within gneissic xenoliths at 1678 ± 14 Ma and 1575 ± 20 Ma respectively using radiogenic $^{207}Pb/^{206}Pb$ dating techniques. This is interpreted as the age of the protolith in the Southern Arunta Inlier (Collins et al., 1995).

Zircon core and rim ages accumulated at 1500-1400 Ma are probably related to the Anmatjira Uplift Phase. This event developed high-strain zones in the Redbank Thrust Zone, generating mineral assemblages that reflect temperatures of 650°C and pressures of 6-7 kbars (Warren & Shaw, 1995). If water were available, amphibolite facies assemblages were developed, however if conditions were dry, granulite facies assemblages were formed. The latter was developed in the Southern Arunta Province (Warren and Shaw, 1995).

The Teapot Granite Complex is the likely source of metamorphism in the southern Arunta Inlier at 1140 Ma (Black & Shaw, 1992a), coinciding with an accumulation of zircon rim ages at 1145 ± 10 Ma in the Heavitree Range Quartzite. The Lower Heavitree Quartzite samples were collected ~1.5 km south of the Teapot Granite Complex. This compares with zircon rim ages obtained from the Chewings Range Quartzite, which pre-date the timing of emplacement of the Teapot Granite Complex. The Chewings Quartzite sample was collected from the southern section of the quartzite ridge, ~5.5 km from the outcropping Teapot Granite Complex to the north. Zircon rim ages were accumulated at ~1600 Ma, which coincide with the age of the Ryans Gap Metamorphics at ~1605 Ma and the emplacement of the Ormiston Pound Granite (Warren & Shaw, 1995). This suggests that localised metamorphism was associated with the emplacement of the Teapot Granite Complex. However further U-Pb zircon rim dating of the northern section of the ridge (closer to heat source) is needed in order to support this metamorphic interpretation.

9.1 Ormiston Gorge cross-sections

The structural cross-sections across the Ormiston region revealed coupled basement and cover deformation along a series of southward verging thrust faults, forming fault propagation style folding (Flottmann & Hand, 1999). However deformation along this interface is difficult to construct in the sub-surface, causing ambiguity in the constructed sections. Thrusts within the northern Heavitree Range Quartzite were interpreted as splay faults of the Ormiston Thrust, dipping steeply to the north to accommodate for horizontal shortening and vertical exhumation estimates provided by Flottmann & Hand (1999). Seismic data collected across the Ormiston region suggests that the Ormiston thrust is a mostly basement-hosted footwall shortcut of the Redbank shear zone, which is exposed 15 km to the north (Flottmann & Hand, 1999).

9.2 Implications for the timing of deformation in the Ormiston region during the Alice Springs Orogeny

Sm-Nd and whole-rock Rb-Sr data collected from the Strangways Ranges, Harts Range Group and the Entia Dome suggest that the Arunta block has remained below 650°C since the Mesoproterozoic (Windrim & McCulloch, 1986; Foden et al., 2005). Further temperature constraints were applied to the southeastern Arunta Inlier by the analysis of $^{40}Ar/^{39}Ar$ hornblende and Rb-Sr muscovite systems, closing to diffusion at about 500 ± 25°C (Dunlap & Teyssier, 1995). This suggests that amphibolite facies conditions were present in the southeastern Arunta block during the early stages of the Alice Springs Orogeny.

Muscovite and minor biotite were accumulated in the Lovely Hill Schist, Glen Helen Metamorphics and the Ryans Gap Metamorphics (Warren & Shaw, 1995), with garnet absent across the Ormiston region. These mineral assemblages represent lower amphibolite facies conditions, which are related to temperatures greater than 350°C. In this study, the closure temperature of muscovite at ~300-350°C (Robbins, 1972; Hames & Bowring, 1994) is considered using $^{40}Ar/^{39}Ar$ dating methods. $^{40}Ar/^{39}Ar$ dating of muscovite from a mylonitic shear zone has provided constraints on the timing of deformation and metamorphism in the Ormiston region. 380 ± 4 Ma is

interpreted as the maximum crystallisation age of muscovite within these shear zones, which means that conditions cooled to ~350°C at a maximum age of 380 ± 4 Ma during the Alice Springs Orogeny.

Sample ORM7 recorded a $^{40}Ar/^{39}Ar$ muscovite age of 350 ± 3 Ma, which is a confident representation of the timing of crystallisation within this shear zone. If peak deformation conditions occurred at 350°C, 350 ± 3 Ma would represent the absolute age of peak deformation in the region. However temperatures exceeded 350°C in the southeastern Arunta Inlier during the Alice Springs Orogeny. Therefore if amphibolite facies conditions were accepted across the Ormiston region, this age would represent the minimum age of peak deformation conditions.

9.3 Key issues and future research

Metamorphic conditions during the Alice Springs Orogeny are poorly constrained, with few low-grade metamorphic studies conducted in the southern Arunta Inlier. The Illite crystallinity method should be considered in low-grade terrains, where the structure of muscovite crystals can be measured. The technique involves the use of an X-ray Diffractometer and can be used to qualitatively measure the following structural features of muscovite crystals:

- Degree of crystallinity
- Size of the crystal
- Stress and strain experienced by the crystal

These factors can provide an insight into the metamorphic conditions (Kubler, 1967; Kisch et al., 2004) that occurred in the Ormiston region during the Alice Springs Orogeny.

10. Conclusion

The main findings of this study are:

- Deposition of the Chewings Quartzite occurred at a maximum age of 1578 ± 21 Ma.
- Deposition in the Amadeus Basin was initiated at a maximum age of 1047 ± 13 Ma, constrained by the basal Pebble Quartzite.
- Greenschist facies conditions were active during the Alice Springs Orogeny, producing muscovite growth in the region.
- Temperatures of 350°C were present at 350 ± 3 Ma, developed in south-verging shear zones across Ormiston Gorge. Shearing was dominantly hydrous, forming mylonites within these deformation zones.
- Peak deformation at Ormiston Gorge occurred at a minimum age of 350 ± 3 Ma, constrained by dating muscovite from within the mylonitic deformed zone.

11. Acknowledgments

First and foremost, I would like to thank my supervisors, Guillaume Backe and Alan Collins for the assistance and guidance they have given me during my 2009 Honours year. Both personnel have answered tireless questions and issues that have arised at different times throughout the year and I appreciate their efforts in doing so. Many thanks must go to the Ormiston Gorge National Park for allowing access to the vast areas of Ormiston Gorge and providing the necessary camping facilities during our stay. Adelaide Microscopy must be thanked, in particular Ben Wade and Angus Netting for their efforts to answer countless questions about the XL20 and LA-ICPMS processes. A special thankyou to Michael Spzunar and Grant Cox for rearranging their schedules to make time available on the LA-ICPMS, given its high demand. Grant must also be thanked for preparing the muscovite samples used for $^{40}Ar/^{39}Ar$ dating. A special thankyou must acknowledge the Honours class of 2009, particularly David Nettle, Frank Robinson, Peter Coleman and Ashlyn Johnson. The Australian Institute of Mining and Metallurgy (AusIMM) in association with Playford Trust are gratefully acknowledged for providing a generous scholarship. My field assistant Quentin cannot go unnoticed for the endless energy sapping walks that were completed in conditions that were not ideal for a Frenchman. Last but no means least, my family must be thanked for their efforts throughout this year, leaving dinner in the oven each night for when I finally decided to come home in the early hours of the morning.

12. References

ANFILOFF, W. & SHAW, R.D., 1973. The gravity effects of three large uplifted granulite blocks in separate Australian shield areas. Proc. Symp. Earth's Gravity Field and Secular Variations in Position, pp. 273-289.

BLACK, L.P. & SHAW, R.D., 1992a. U-Pb zircon chronology of prograde Proterozoic events in the Central and Southern Provinces of the Arunta Block, central Australia. *Australian Journal of Earth Sciences* **39**, 153-171.

BLACK, L.P. & SHAW, R.D. 1992b. The status of Rb-Sr dating in the derivation of Arunta Inlier geochronology. In: The application of geochronology to field-related geological problems. Geological Society of Australia SGGMP Worksop, Alice Springs, July 5-11, 1992.

BLACK, L.P. & SHAW, R.D., 1995. An assessment, based on U-Pb zircon data, of Rb-Sr dating in the Arunta Inlier, central Australia. In: Time limits on tectonic events and crustal evolution using gechronology: some Australian examples. (edited by Collins, W.J. and Shaw, R.D.). *Precambrian Research* **71**, 3-15.

BLACK, L.P., SHAW, R.D. & STEWART, A.J., 1983. Rb-Sr geochronology of Proterozoic events in the Arunta Inlier, central Australia. Australian Bureau of Mineral Resources, *Journal of Geology and Geophysics* **8**, 129-137.

CAMACHO, A., COMPSTON, W., McCULLOCH, M. & McDOUGALL, I., 1997. Timing and exhumation of eclogite facies shear zones, Musgrave Block, central Australia. *Journal of Metamorphic Geology* **15**, 735-751.

COLLINS, W.J. & SHAW, R.D., 1995. Geochronological constraints on tectonic events in the Arunta Inlier; a review. In: Time limits on tectonic events and crustal evolution using geochronology: some Australian examples. (edited by Collins, W.J. and Shaw, R.D.). *Precambrian Research* **71**, 315-346.

COLLINS, W.J., WILLIAMS, I.S., SHAW, S.E. & McLAUGHLIN, N.A., 1995. The age of the Ormiston Pound Granite: implications for Mesoproterozoic evolution of the Arunta Inlier, central Australia. *Precambrian Research* **71**, 91-105.

DUNLAP, J.W. & TEYSSIER, C., 1995. Paleozoic deformation and isotopic disturbance in the southeastern Arunta Block, central Australia. *Precambrian Research* **71**, 229-250.

FLOTTMANN, T. & HAND, M., 1999. Folded basement-cored tectonic wedges along the northern edge of the Amadeus Basin, central Australia: evaluation of orogenic shortening. *Journal of Structural Geology* **21**, 399-412.

FODEN, J., MAWBY, J., KELLEY, S., TURNER, J.P. & BRUCE, D., 1995. Metamorphic events in the eastern Arunta Inlier, Part 2. Nd-Sr-Ar isotopic constraints. In: Time Limits on Tectonic Events and Crustal Evolution Using Geochronology: Some Australian Examples. *Precambrian Research* **71**, 207-227.

GILLAM, D.J., 2005. Structural and geomechanical analysis of naturally fractured hydrocarbon provinces of the Bowen and Amadeus Basins: Onshore Australia. Australian. Thesis (Ph.D.). University of Adelaide. Australian School of Petroleum.

HAINES, P.W., HAND, M. & SANDIFORD, M., 2001. Palaeozoic synorogenic sedimentation in central and northern Australia; a review of distribution and timing with implications for the evolution of intracontinental orogens. *Australian Journal of Earth Sciences* **48**(6), 911-928.

HAMES, W.E., & BOWRING, S.A., 1994. An empirical evaluation of the argon diffusion geometry in muscovite. *Earth and Planetary Science Letters* **124**, 161-167.

HAND, M. & SANDIFORD, M., 1999. Intraplate deformation in central Australia, the link between subsidence and fault reactivation. *Tectonophysics* **305**, 121-140.

HARRISON, T.M. & ZEITLER, P.K., 2005. Fundamentals of noble gas thermochronometry. (edited by Reiners, P.W. & Ehlers, T.A.). Low temperature thermochronology: techniques, interpretaions and applications, *Reviews in Mineralogy and Geochemistry* **58**, 123-149.

JACKSON, S.E., PEARSON, N.J., GRIFFIN, W.L. & BELOUSOVA, E.A., 2004. The application of laser ablation-inductively coupled plasma-mass spectrometry to in situ U-Pb zircon geochronology. *Chemical Geology* **211**(1-2), 47-69.

KISCH, H.J., ARKAI, P. & BRIME, C., 2004. On the calibration of the illite Kubler Index (illite "crystallinity). *Schweizerische Mineralogische und Petrographische Mittereilungen* **84**, 323-331.

KOPPERS, A.A.P., 2002. ArArCALC-software for 40Ar/39Ar age calculations. *Computers & geosciences* **28**, 605-619.

KORSCH, R.J. & LINDSAY, J.F., 1989. Relationships between deformation and basin evolution in the intracratonic Amadeus Basin, central Australia. *Tectonophysics* **158**, 5-22.

KUBLER, B., 1967. La cristallinite de I'illite et les zones tout a fait superieures de metamorphisme. In: Colloque sur les etages tectoniques (edited by Schaer, J.P.). *A la Baconniere, Neuchatel*, 105-112.

LANPHERE, M.A. & DALRYMPLE, G.B., 1976. Identification of excess 40Ar by the 40Ar/39Ar age spectrum technique. *Earth and Planetary Science Letters* **32**, 141-148.

LINDSAY, J.F., 1999. Heavitree Quartzite, a Neoproterozoic (ca. 800-760 Ma) high-energy, tidally influenced, ramp association, Amadeus Basin, central Australia. *Australian Journal of Earth Sciences* **46**, 127-139.

LINDSAY, J.F. & KORSCH, R.J., 1991. The evolution of the Amadeus Basin, central Australia. (edited by Korsch, R.J. & Kennard, J.K.). Bureau of Mineral Resources Bulletin 236: Geological and Geophysical Studies in the Amadeus Basin, Central Australia, p. 7-32.

LIU, S.F., RAYMOND, O.L., STEWART, A.J., SWEET, I.P., DUGGAN, M., CHARLICK, C., PHILLIPS, D., RETTER, A.J., 2006. Surface geology of Australia 1:1,000,000 scale, Northern Territory – 1st edition [digital dataset]. Canberra: The Commonwealth of Australia, Geoscience Australia.

MARJORIBANKS, R.W., 1976. Basement and cover relations on the northern margin of the Amadeus Basin, central Australia. *Tectonophysics* **33**, 15-32.

MARJORIBANKS, R.W. & BLACK, L.P., 1974. Geology and geochronology of the Arunta Complex, north of Ormiston Gorge, central Australia. *Journal of the Geological Society of Australia* **21**, 291-299.

McLAUGHLIN, N.A., 1994. The Proterozoic Geology of Ormiston Pound: implications for the tectonic evolution of the Southern Arunta Province. B.Sc (Hons) Thesis, Department of Geology, University of Newcastle.

OBEE, H.K. & WHITE, S.H., 1985. Faults and associated fault rocks of the Southern Arunta block, Alice Springs, central Australia. *Journal of Structural Geology* **7**(6), 701-712.

RAIMONDO, T., COLLINS, A., HAND, M., WALKER-HALLAM, A., SMITHIES, H.R., EVINS, P.M. & HOWARD, H.M., 2009. Ediacaran intracontinental channel flow. *Geological Society of America* **37**(4), 291-294.

ROBBINS, G.E., 1972. Radiogenic argon diffusion in muscovite under hydrothermal conditions. M.S. Thesis, Brown University. Providence, Rhode Island.

SCRIMGEOUR, I. & CLOSE, D., 1998. Regional high-pressure metamorphism during intracratonic deformation: the Petermann Orogeny, central Australia. *Journal of Metamorphic Geology*.

SHAW, R.D. & BLACK, L.P., 1991. The history and tectonic implications of the Redbank thrust zone, central Australia, based on structural, metamorphic and Rb-Sr isotopic evidence. *Australian Journal of Earth Sciences* **38**(3), 307-332.

SHAW, R.D., ZEITLER, P.K., McDOUGALL, I. and TINGATE, P.R., 1992. The Paleozoic history of an unusual intracratonic thrust belt in central Australia based on 40Ar-39Ar, K-Ar and fission track dating. *Journal of the Geological Society of London* **149**, 937-954.

SOUTHGATE, P.N., 1991. A sedimentological model for the Loves Creek Member of the Bittersprings Formation, northern Amadeus Basin. In R.J. Korsch and J.K. Kennard, eds., Bureau of Mineral Resources Bulletin 236: Geological and geophysical studies in the Amadeus Basin Central Australia, p. 113-126.

STEIGER, R.H., JAGER, E., 1977. Subcommission on geochronology: convention on the use of decay constants in geo- and cosmochronology. *Earth and Planetary Science Letters* **36**, 359-362.

TEYSSIER, C., 1985. A crustal thrust system in an intracratonic tectonic environment. *Journal of Structural Geology* **7**, 689-700.

TINGATE, P.R., 1991. Apatite fission track analysis of the Pacoota and Stairway Sandstones, Amadeus Basin, central Australia. (edited by Korsch, R.J. and Kennard, J.K). Bureau of Mineral Resources Bulletin 236: Geological and Geophysical Studies in the Amadeus Basin Central Australia, p. 525-541.

VAN ACHTERBERGH, E., RYAN, C.G., JACKSON, S.E. & GRIFFIN, W.L., 2001. Data reduction software for LA-ICPMS. In: Laser-ablation-ICPMS in the earth sciences; principles and applications. (edited by Paul, J.S.). Mineralogical Association of Canada, Ottowa, ON, Canada.

WADE, B. P., HAND, M. & BAROVICH, K.M., 2005. Nd isotopic and geochemical constraints on provenance of sedimentary rocks in the eastern Officer Basin, Australia: implications for the duration of the intracratonic Petermann Orogeny. *Journal of the Geological Society of London* **162**, 513-530.

WALTER, M.R., VEEVERS, J.J., CALVER, C.R. & GREY, K., 1995. Neoproterozoic stratigraphy of the Centralian Superbasin, Australia. *Precambrian Research* **73**, 173-195.

WARREN, R.G. & SHAW, R.D., 1995. Hermannsburg SF 53-13, Northern Territory: Northern Territory Geological Survey, 1:250 000 Geological Map Series Explanatory Notes.

WINDRIM, D., & McCULLOCH, M.T., 1986. Nd and Sr isotopic systematics of central Australian granulites: Chronology of crustal development and constraints on the evolution of lower continental crust. Contributions to Mineral Petrology **94**, 289-303.

ZHAO, J.X., McCULLOCH, M.T. & COMACHO, A., 1992. Geochemical and isotopic studies of Proterozoic mafic dyke swarms in central Australia. *Geological Society of Australia Abstract* **32**, 205-207.

13. Figure captions

Figure 1. A regional map of Ormiston Gorge showing the position of the cross-sections constructed in this study. The cross-section produced along the Mount Sonder section represents previous studies by Flotmann and Hand (1999). In the east of the map, the section traces across Ormiston Gorge are classified as follows: C-D = west of Ormiston Gorge section; E-F section trace = Ormiston Gorge section; G-H = Back Gorge section; I-J = Ormiston Pound section.

Figure 2; Field map constructed across the Ormiston region. South-propagating thrusts are characteristic across the northern margin of the Amadeus Basin, forming a series of thrusts within the Ormiston thrust zone. Thrust faulting within the Heavitree Range Quartzite is accompanied by overturned anticline-syncline pairs developed in the footwall of the Ormiston thrust.

Figure 3. The western mapping area of Ormiston Gorge. Lower Heavitree Quartzite overlies the Ormiston Pound Granite in the east of the mapping area. This contact is interpreted as a thrust due to the development of mylonitic shear fabric observed in the Back Gorge. The Upper Heavitree Quartzite conformably overlies the massive quartzite beds with a repeated unit of Lower Heavitree Quartzite overlying the sequence along a thrust fault contact. Folding in the region was revealed in the south of map with the erosional remnants of an east-west trending anticline observed within the Bittersprings cover sequence. The Lower and Upper Heavitree Quartzites occupy the core of the anticline, which outcrops to the south of the Ormiston Gorge campgrounds.

Figure 4. The northeastern mapping area of Ormiston Gorge illustrates the north-south striking Chewings Range Quartzite (green unit). This ridge forms the eastern margin of the Ormiston Pound, associated with a prominent east-dipping foliation (Chewings Orogeny). Heavitree Quartzite sediments unconformably overlying part of

the northern Chewings Range Quartzite were associated with an east-west trending overturned syncline developed during the Alice Springs Orogeny.

Figure 5. Looking towards the western edge of Ormiston Gorge, where the Heavitree Quartzite Range has been thrust southward during the Alice Springs Orogeny; (a) The Lower Heavitree Quartzite beds are represented by the prominent cliff faces seen in this image, which overly basement rocks of the Ormiston Pound Granite. The Lower Heavitree Quartzite beds are also present at the top of this quartzite range, with the Upper Heavitree Quartzite beds occupying the vegetated area in between. (b) The units have been annotated on this diagram with the Ormiston Pound Granite represented in blue at the base of the image, followed by the orange and pink bedding of the Lower and Upper Heavitree Quartzites respectively. The repeated Lower Heavitree Quartzite beds which overly the Upper Heavitree Quartzite were uplifted during south-verging thrust faulting during the Alice Springs Orogeny; (c) The Lower Heavitree Quartzite beds illustrated vary in thickness from 0.1-2 m. These massive sand beds are associated with brittle deformation, which is evident from the high concentration of fractures seen in the outcrop; (d) Horses developed in the Lower Heavitree Quartzite. These structures indicate north over south movement across Ormiston Gorge; (e) Overturned folds are illustrated in the Ormiston Pound Granite. The red lines have been used to trace the limbs of the folds, revealing a short southern limb and a long northern limb. This is the result of north-south compression across this region during the Alice Springs Orogeny; (f) Mica-fish structure developed in the Heavitree Quartzite seen at the Back Gorge. This structure indicates top to the south.

Figure 6. Axial plane data collected across the area. The axial plane moderately dips to the north, which is likely to reflect north-south compression in the region during the Alice Springs Orogeny.

Figure 7. Lineation data collected from the Lower and Upper Heavitree Quartzites, indicating movement in a north-south orientation. The direction of movement is interpreted from kinematic indicators found in this area, which suggest north over south movement.

Figure 8. Foliation data collected from Ormiston Pound, expressed on the geological map of Ormiston Gorge.

Figure 9. Comparison of bedding measurements across the Ormiston Gorge region for each geological unit; (a) All bedding measurements recorded in the western area of Ormiston Gorge. The beds trend east-west with fold hinges plunging shallowly to the west (β); (b) Lower Heavitree Quartzite bedding readings in the western mapping area; (c) Upper Heavitree Quartzite bedding data; (d) Bittersprings Formation bedding data; (e) Heavitree Quartzite bedding measurements recorded from isolated outcrop, which unconformably overlies part of the northern Chewings Range Quartzite ridge. These beds moderately dip to the north, representing an east-west trending overturned syncline in the quartzite.

Figure 10. Fold hinge measurements taken in the Lower and Upper Heavitree Quartzite plunge to west. This is consistent with the β-measurements obtained from the bedding data in the west of the area.

Figure 11. Diagrammatic representation of LA-ICPMS zircon age data obtained from sample 40A_PQ; (a) Illustrates the internal structure of the detrital zircons dated in this sample. The zircons reveal some growth zoning, with spot 24 and 29 representing zircon cores ages; (b) U-Pb zircon age data is plotted on the concordia diagram for all zircons in the sample with 90-110% concordance. Black ellipses represent the age and error associated with each zircon analysed. Inset: Probability density plot of all zircons included in the concordia plot; (c) U-Pb plot of zircon core ages with 90-110% concordance. Cores were identified using the SEM images. Inset: Probability density plot of the zircon core ages; (d) Zircon rims with 90-110% concordance are plotted on the U-Pb concordia plot. Rims identified from analysing the SEM images. Inset: Probability density plot of the zircon rim ages.

Figure 12. Diagrammatic representation of LA-ICPMS zircon age data obtained from sample 40C_LHTQ; (a) Illustrates the area of some of the zircons targeted. Growth zoning is common in this sample, however zircon cores including spot 64 are also accumulated in the Neoproterozoic sediments and are commonly dated at ~1600 Ma; (b) Conventional U-Pb concordia plot of all zircon age data. Black ellipses represent the age and error associated with each zircon analysed. Inset: Probability density plot

of all zircons included in the concordia plot with concordance between 90% and 110%; (c) Zircon core ages with 90-110% concordance are plotted on the U-Pb concordia diagram. Inset: Probability density plot of the zircon core ages. Cores were identified from the SEM images and targeted if possible to interpret the source of the zircon; (d) Zircon rim ages are plotted on the U-Pb concordia diagram with 90-110% concordance. Rims were identified from the SEM images. Inset: Probability density plot of the zircon rim ages.

Figure 13. Diagrammatic representation of LA-ICPMS zircon age data obtained from sample 34B_CQ; (a) SEM images illustrating the area of the zircon targeted; (b) U-Pb concordia age plot of all zircons analysed. Black ellipses represent the age and error associated with each zircon analysed. Inset: Probability density plot of all zircon age data with 90-110% concordance; (c) Zircon core ages between 90-110% concordance were plotted on the U-Pb concordia age plot. The zircon cores were identified using the SEM images collected prior to age analysis. Inset: Probability density plot of the zircon core ages.

Figure 14. Diagrammatic representation of ^{40}Ar-^{39}Ar ages obtained from muscovite extracted from within a mylonitic shear zone (sample ORM7); (a) Age plateau of sample, producing a plateau age of 350 ± 3 Ma over 11 consecutive steps of cumulative ^{39}Ar released (%); (b) Normal Isochron age plot, recording a normal isochron age of 347 ± 8 Ma; (c) Illustrates the internal structure of a selection of zircons accumulated in the Chewings Range Quartzite. Spots 5 and 34 represent zircon zoned cores, which are surrounded by prominent growth zoning. Spots 10, 31 and 52C reflect fragments of growth zoning.

Figure 15. Diagrammatic representation of ^{40}Ar-^{39}Ar muscovite ages obtained from sample ORM8; (a) Age plateau produced over 4 consecutive steps of cumulative ^{39}Ar released (%), producing a U-shape age plot; (b) Normal isochron plot. A normal isochron age could not be obtained due to the presence of excess argon in this sample, indicated by the U-shape developed in (a).

Figure 16. Section trace across the Mount Sonder area showing the downward facing Razorback structure (Flottmann & Hand, 1999). Points C and D represent the northern and southern endpoints of the cross-section constructed in Figure 14.

Figure 17. Sequentially restored cross-section across the Mount Sonder area (Flottmann & Hand, 1999). The horizontal arrows on right indicate the amount of orogenic shortening in kilometers; (a) Balanced cross-section illustrating the final deformation geometry across the Mount Sonder region. In order to balance the section, erosion of topography is presumed to source the sediments deposited in the foreland basin; (b) Section expresses the initial southward tilt of the proto-Razorback structure; (c) Proto-Razorback structure developed in an intercutaneous wedge mainly confined to the Bittersprings Formation. Rotation of the wedge in (a) and (b) has been caused by footwall shortcut thrusts, developing basement-cored folds; (d) Restored cross-section across Mount Sonder (refer to Figure 19 for legend).

Figure 18. Section trace across the Ormiston Gorge area constructed along two traces (Flottmann & Hand, 1999). The northern and southern endpoints are labeled A and B and were used to construct the cross-section shown in Figure 19.

Figure 19. (a) Cross-section across the Ormiston Gorge area, where points A and B represent the endpoints of the section trace; (b) Restored section of the Ormiston Gorge area, using the Ormiston Thrust as a loose line (Flottmann and Hand, 1999).

Figure 20. The cross-section constructed west of Ormiston Gorge reveals basement-rooted southward-propagation thrusts, which penetrate the overlying Heavitree Range Quartzite. These beds have also been folded with the development of overturned anticline-syncline pairs in the footwall of the Mesoproterozoic Ormiston thrust.

Figure 21. A series of basement-rooted splay faults have been generated in the footwall of the Ormiston thrust. This cross-section illustrates the formation of a southward-verging duplex structure across Ormiston Gorge, also highlighting intense folding in the region associated with the basement and overlying cover sequence.

Figure 22. The Back gorge section reveals south propagating thrust zones within the Heavitree Range Quartzite along interpreted splay faults of the Ormiston thrust. The Lower Heavitree Quartzite beds observed at the top of the Heavitree Range have been thrust on top of the Upper Heavitree Quartzite.

Figure 23. The Ormiston Pound section expresses coupled basement and cover deformation, with the formation of overturned anticline-syncline pairs identified previously (Warren & Shaw, 1995). The disharmonic nature of the Bittersprings Formation is well illustrated in this section, with deformation constrained to the top of the Heavitree Range.

Tectonic evolution summary of central Australia (refined from Collins and Shaw, 1995; Dunlap & Teyssier, 1995)

Age (Ma)	Northern Tectonic province	Central tectonic province	Southern Tectonic province	Revised nomenclature
>1880	Yuendumu tectonic event			Yuendumu Tectonic Event
1860-1820	Mount Stafford tectonic phase			Stafford Tectonic Event
1820-1780	Reynolds assemblage deposition	Reynolds assemblage deposition		
1780-1770	Weldon tectonic phase	Ongeva phase		First phase of Strangways Orogeny
1745-1730		Pfitzner phase; Wuluma phase; Harts Range orogeny		Second phase of Strangways Orogeny
1670-1660			Igneous activity; migmatisation; deformation	Argilke Tectonic Event
~1600	Pegmatite intrusion; granitoid intrusion		North-directed thrusting granitoid sheet intrusion	Chewings Orogeny
1500-1400	Shearing?		South-directed shearing along the Redbank shear zone	Anmatjira Uplift Phase
1200-1100			Teapot Granite emplacement and pegmatites	Teapot Magmatic Event
1050	Dolerite dyke intrusion	Major uplift and shearing		Extension?
400-300	South-directed thrusting	South-drected thrusting		Alice Springs Orogeny

LA-ICPMS analyses used for U-Pb dating of zircons

Sample 40A_PQ

						Age (Ma)	
Zircon Grain	**Location**	**Pb207/U235**		**Pb206/U238**		**Pb206/U238**	**Pb207/Pb206**
SPOT1	Structureless	3.59848	0.05138	0.26947	0.00373	1538.1 ± 18.97	1564.3 ± 20.48
SPOT3	Zoning	3.03264	0.0469	0.24484	0.00363	1411.8 ± 18.81	1422.7 ± 22.44
SPOT4	Structureless	1.91174	0.03336	0.17625	0.00245	1046.5 ± 13.4	1164.5 ± 31.51
SPOT5	Zoned Core	3.19721	0.04591	0.24582	0.00328	1416.9 ± 16.97	1515.5 ± 22.68
SPOT6	Zoning	2.08506	0.0406	0.19408	0.00277	1143.4 ± 14.95	1146.5 ± 36.51
SPOT7	Zoning	1.9665	0.03749	0.18922	0.00267	1117.1 ± 14.46	1080.1 ± 35.96
SPOT10	Zoning	3.85741	0.05998	0.28819	0.00396	1632.5 ± 19.82	1569.4 ± 25.22
SPOT11	Zoned Core (inclusion evident)	3.72694	0.05667	0.26814	0.00368	1531.3 ± 18.72	1639.2 ± 23.97
SPOT12	Structureless	3.56287	0.05368	0.26977	0.00366	1539.6 ± 18.6	1543.9 ± 24.14
SPOT13	Structureless	2.18659	0.05036	0.20625	0.00346	1208.8 ± 18.47	1118.8 ± 42.06
SPOT14	Structureless	3.24348	0.04536	0.24848	0.00336	1430.6 ± 17.36	1521.7 ± 20.87
SPOT15	Probable Zoned Core	3.52589	0.07164	0.26642	0.00397	1522.6 ± 20.18	1548 ± 36.55
SPOT16	Zoned Core	3.68074	0.05392	0.27027	0.00368	1542.2 ± 18.67	1601.3 ± 22.62
SPOT17	Zoning	3.78331	0.05674	0.27409	0.00381	1561.5 ± 19.28	1626.5 ± 22.86
SPOT19	Rim	2.57218	0.03833	0.21599	0.00295	1260.6 ± 15.62	1346.8 ± 23.99
SPOT20	Core and Zoning	2.34533	0.04998	0.20326	0.00317	1192.8 ± 16.99	1285.2 ± 38.67
SPOT22	Zoned Core	3.68004	0.05163	0.27306	0.00365	1556.3 ± 18.48	1581.5 ± 21.26
SPOT23	Zoning	2.14322	0.0354	0.19534	0.00275	1150.3 ± 14.82	1186.3 ± 28.22
SPOT24	Zoned Core	3.72082	0.05765	0.27693	0.00394	1575.9 ± 19.9	1575.6 ± 23.38
SPOT25	Zoned Core	3.5406	0.05164	0.26544	0.00357	1517.6 ± 18.19	1562.1 ± 22.85
SPOT26	Zoned Core	5.06226	0.07477	0.32699	0.00445	1823.8 ± 21.62	1836.6 ± 22.43
SPOT27	Zoned Core	3.8231	0.05854	0.27816	0.00383	1582.1 ± 19.32	1618 ± 24.1
SPOT28	Structureless	2.16421	0.04837	0.19564	0.00298	1151.9 ± 16.08	1203 ±42.28
SPOT29	Zoned Core	3.69021	0.06858	0.27595	0.00399	1570.9 ± 20.17	1567 ± 32.6
SPOT30	Rim	2.10364	0.05286	0.19399	0.00307	1142.9 ± 16.57	1163.5 ± 48.94
SPOT32	Zoned Core	3.29407	0.05005	0.24557	0.0035	1415.6 ± 18.13	1571.1 ± 22.44
SPOT33	Zoned Core	3.24035	0.04778	0.2478	0.00351	1427.1 ± 18.12	1523.2 ± 21.34
SPOT36	Probable Core	3.68981	0.07503	0.27233	0.00412	1552.6 ± 20.87	1591.9 ± 35.92
SPOT36RM	Rim	3.40757	0.0659	0.25796	0.00381	1479.4 ± 19.53	1544.3 ± 33.92
SPOT39	Zoning	3.68887	0.0598	0.26849	0.00385	1533.1 ± 19.54	1618.8 ± 24.88
SPOT40	Structureless	3.97481	0.07525	0.27476	0.00418	1564.9 ± 21.11	1713.8 ± 31.08
SPOT41	Rim	3.41141	0.0562	0.25383	0.00401	1458.2 ± 20.6	1579.1 ± 22.77
SPOT42	Zoned Core	2.97601	0.04445	0.24313	0.00369	1402.9 ± 19.15	1400.6 ± 19.69
SPOT44	Zoning	2.40952	0.06139	0.21165	0.00372	1237.6 ± 19.78	1263.5 ± 47.34
SPOT45	Zoning	2.27637	0.03653	0.20606	0.00297	1207.8 ± 15.89	1199.9 ± 25.34
SPOT47	Zoned Core	4.19372	0.07418	0.297	0.00474	1676.4 ± 23.57	1673.1 ± 26.9
SPOT48	Structureless	2.03199	0.02834	0.1877	0.00248	1108.9 ± 13.45	1160.2 ± 22.63
SPOT49	Rim	3.75551	0.05545	0.27894	0.00374	1586 ± 18.87	1580 ± 23.54
SPOT50	Zoning	2.15003	0.03341	0.19888	0.00263	1169.3 ± 14.13	1158.1 ± 27.37
SPOT51	Structureless	3.80541	0.05873	0.28281	0.0038	1605.5 ± 19.11	1579.2 ± 25.47
SPOT52	Zoned Core	3.62247	0.04943	0.27149	0.00361	1548.4 ± 18.3	1563 ± 20.35
SPOT53	Zoning	3.74046	0.05209	0.2664	0.00358	1522.5 ± 18.21	1658.2 ± 20.68

SPOT54	Structureless	4.43536	0.06353	0.30732	0.00417	1727.5 ± 20.55	1709 ± 21.5
SPOT55	Zoned Core	3.83039	0.05461	0.27909	0.00377	1586.8 ± 18.98	1615.8 ± 21.63
SPOT56	Fracture Fill and Zoning	3.5641	0.05003	0.26626	0.00343	1521.8 ± 17.49	1569.2 ± 22.42
SPOT57	Structureless	3.8817	0.05585	0.27698	0.00386	1576.1 ± 19.48	1654.2 ± 20.96
SPOT58	Zoning	3.68527	0.0556	0.27368	0.00388	1559.4 ± 19.65	1579.8 ± 22.73
SPOT59	Rim	2.23891	0.0522	0.19664	0.00314	1157.2 ± 16.93	1259.3 ± 43.55
SPOT60	Structureless	4.05151	0.08105	0.28004	0.00437	1591.6 ± 22	1712.9 ± 34.18
SPOT61	Rim	2.2218	0.04004	0.19951	0.00291	1172.7 ± 15.64	1215.1 ±31.35
SPOT62	Structureless	3.59025	0.05107	0.26408	0.00362	1510.7 ± 18.48	1597.5 ± 20.75
SPOT63	Structureless	3.34015	0.04607	0.24985	0.00342	1437.7 ± 17.62	1566.1 ± 19.5
SPOT64	Structureless	2.27635	0.03539	0.20244	0.00285	1188.4 ± 15.26	1233.7 ± 25
SPOT65	Structureless	2.10245	0.03116	0.19421	0.0027	1144.1 ± 14.55	1158.8 ± 23.37
SPOT66	Structureless	3.38696	0.04712	0.25215	0.00338	1449.6 ± 17.41	1574.8 ± 20.58
SPOT67	Structureless	3.85551	0.05728	0.28239	0.00392	1603.4 ± 19.69	1604.9 ± 22.25

Sample 40C_LHTQ

						Age (Ma)	
Zircon Grain	**Location**	**Pb207/U235**		**Pb206/U238**		**Pb206/U238**	**Pb207/Pb206**
SPOT1	Rim	2.39284	0.03944	0.21087	0.00278	1233.5 ± 14.81	1252.1 ± 30.18
SPOT2	Structureless	4.11135	0.07429	0.29667	0.00412	1674.8 ± 20.5	1634.6 ± 31.93
SPOT3	Rim	2.44755	0.05104	0.21424	0.00301	1251.4 ± 15.96	1266.1 ± 39.44
SPOT4	Structureless	4.19609	0.07288	0.29722	0.00412	1677.5 ± 20.49	1667.1 ± 30.78
SPOT6	Core	3.64161	0.05873	0.27831	0.00377	1582.9 ± 19	1525.1 ± 28.4
SPOT7	Zoning	3.84903	0.05999	0.28662	0.00386	1624.6 ± 19.35	1573.8 ± 26.94
SPOT9	Structureless	4.65281	0.07118	0.31186	0.00414	1749.9 ± 20.36	1769.8 ± 25.12
SPOT10	Core	2.42474	0.04511	0.219	0.00307	1276.6 ± 16.24	1203.5 ± 34.81
SPOT12	Structureless	3.74464	0.05137	0.27528	0.00355	1567.6 ± 17.94	1598.3 ± 22.24
SPOT13	Zoning	2.48845	0.0367	0.21577	0.00287	1259.5 ± 15.24	1283.6 ± 25.47
SPOT15	Rim	3.50271	0.05652	0.27848	0.00378	1583.7 ± 19.04	1452.6 ± 28.04
SPOT16	Rim	2.43016	0.03654	0.22095	0.00289	1286.9 ± 15.28	1191.1 ± 26.61
SPOT17	Zoning	3.57669	0.05552	0.28072	0.0037	1595 ± 18.64	1476.5 ± 26.9
SPOT18	Zoning	4.04519	0.06261	0.30357	0.00402	1709 ± 19.87	1562.3 ± 26.51
SPOT22	Zoning	5.07233	0.09222	0.32452	0.00451	1811.7 ± 21.95	1857.9 ± 30.41
SPOT24	Zoning	2.55289	0.04807	0.21863	0.00301	1274.6 ± 15.94	1312.9 ± 33.94
SPOT25	Zoned Core	3.94149	0.06852	0.28528	0.00392	1617.9 ± 19.66	1632.5 ± 29.45
SPOT26	Zoning	3.65322	0.07237	0.27571	0.00388	1569.7 ± 19.63	1554.5 ± 34.81
SPOT27	Possible Core	4.16106	0.08666	0.2853	0.0041	1618 ± 20.57	1732.8 ± 36.06
SPOT31	Structureless	4.08089	0.06291	0.29437	0.00389	1663.3 ± 19.37	1633.8 ± 26.23
SPOT32	Structureless	4.09632	0.0648	0.2978	0.00402	1680.4 ± 19.95	1619.3 ± 27.46
SPOT33	Zoning	4.23095	0.06131	0.30372	0.00399	1709.7 ± 19.74	1644 ± 24.27
SPOT34	Zoning	4.28991	0.06939	0.29835	0.00403	1683.1 ± 20.02	1701.2 ± 27.45
SPOT36	Rim	3.62865	0.06461	0.27457	0.00384	1563.9 ± 19.44	1544.4 ± 32.4
SPOT37	Structureless	3.95689	0.05937	0.2949	0.00394	1666 ± 19.61	1574.4 ± 25.48
SPOT38	Structureless	4.32548	0.11572	0.29909	0.005	1686.8 ± 24.82	1711.8 ± 48.96
SPOT39	Rim	2.41802	0.04124	0.21006	0.00284	1229.1 ± 15.13	1278.3 ± 30.73
SPOT40	Zoning	5.0113	0.07291	0.33187	0.00439	1847.5 ± 21.26	1794.3 ± 24.62
SPOT41	Zoning	2.91673	0.04767	0.23796	0.00318	1376.1 ± 16.58	1403.7 ± 29.14
SPOT42	Structureless	4.25813	0.08743	0.28722	0.0043	1627.6 ± 21.53	1770.9 ± 37.76
SPOT43	Possible Core	4.41729	0.08297	0.30687	0.00442	1725.3 ± 21.78	1712.9 ± 34.1
SPOT44	Structureless	4.67753	0.10251	0.32008	0.00485	1790.1 ± 23.66	1744.6 ± 41.45
SPOT45	Zoning	4.24817	0.12611	0.30465	0.0044	1714.3 ± 21.72	1642.8 ± 64.42
SPOT47	Rim	2.74394	0.05293	0.23919	0.00328	1382.5 ± 17.06	1274 ± 38.83
SPOT51	Structureless	4.28868	0.09676	0.29977	0.00437	1690.2 ± 21.65	1692.4 ± 45.68
SPOT52	Structureless	4.52454	0.09678	0.31058	0.00431	1743.6 ± 21.19	1727.1 ± 44.48
SPOT53	Zoning	4.51646	0.1078	0.30817	0.00453	1731.7 ± 22.34	1735.7 ± 48.49
SPOT54	Rim	3.44675	0.09774	0.26531	0.00386	1517 ± 19.68	1515.3 ± 60.56
SPOT55	Structureless	4.60763	0.11183	0.31115	0.00449	1746.4 ± 22.07	1759 ± 51.39
SPOT56	Zoning	2.41668	0.04385	0.21633	0.00293	1262.4 ± 15.53	1220.7 ± 36.08
SPOT57	Zoning	4.49722	0.08852	0.30712	0.00423	1726.5 ± 20.86	1732.7 ± 38.62
SPOT58	Zoning	3.8212	0.06802	0.28101	0.00376	1596.4 ± 18.93	1593.6 ± 35.25
SPOT59	Structureless	5.61272	0.11927	0.34536	0.00459	1912.4 ± 21.98	1931.3 ± 45.11
SPOT60	Core	4.29926	0.08672	0.30171	0.00404	1699.8 ± 20	1688.5 ± 42.2
SPOT61	Structureless	3.89174	0.06057	0.28355	0.00377	1609.2 ± 18.95	1615.3 ± 26.56

SPOT62	Possible Rim	2.28198	0.04694	0.20589	0.00292	1206.9 ± 15.62	1206.5 ± 39.22
SPOT63	Zoning	4.2144	0.06184	0.29719	0.00383	1677.3 ± 19.04	1677.8 ± 24.73
SPOT64	Core	4.00852	0.05704	0.28194	0.00353	1601.1 ± 17.73	1685.1 ± 24.2
SPOT65	Structureless	4.29124	0.06964	0.3012	0.00404	1697.2 ± 20.04	1684.4 ± 27.8
SPOT66	Zoning	3.93518	0.05192	0.28761	0.0036	1629.6 ± 18.01	1611.6 ± 21.4
SPOT67	Structureless	2.0379	0.03228	0.18732	0.00241	1106.8 ± 13.09	1171.7 ± 29.12
SPOT68	Structureless	4.08422	0.05704	0.29592	0.00376	1671 ± 18.69	1627.3 ± 23.26
SPOT71	Zoned Core	4.17615	0.06146	0.29223	0.00377	1652.7 ± 18.8	1692.3 ± 24.64

Sample 34B_CQ

						Age (Ma)	
Zircon Grain	**Location**	**Pb207/U235**		**Pb206/U238**		**Pb206/U238**	**Pb207/Pb206**
SPOT1	Zoned Core	4.53474	0.08089	0.30268	0.00474	1704.6 ± 23.45	1777.6 ± 26.74
SPOT2	Zoning	4.58568	0.06908	0.31177	0.00453	1749.4 ± 22.27	1743.5 ± 20.58
SPOT3	Structureless	4.13966	0.08959	0.29466	0.00496	1664.8 ± 24.69	1659.3 ± 36.13
SPOT4	Core	4.70701	0.08005	0.3182	0.00478	1781 ± 23.4	1753.9 ± 25.72
SPOT5	Zoning	4.50166	0.07431	0.30788	0.00457	1730.3 ± 22.51	1732.7 ± 24.64
SPOT6	Zoning	4.00481	0.06023	0.28792	0.00411	1631.1 ± 20.59	1640.6 ± 21.44
SPOT7	Structureless	4.00677	0.06569	0.28167	0.00442	1599.8 ± 22.21	1681.5 ± 22.24
SPOT8	Structureless	4.82503	0.0794	0.32198	0.00494	1799.4 ± 24.09	1778.1 ± 23.1
SPOT9	Structureless	4.44917	0.06657	0.30542	0.00442	1718.1 ± 21.81	1725.9 ± 20.41
SPOT10	Zoning	3.82613	0.06437	0.2813	0.00439	1597.9 ± 22.09	1599.4 ± 24.26
SPOT11	Zoning	4.05911	0.06231	0.29157	0.00418	1649.4 ± 20.85	1642.7 ± 22.32
SPOT12	Zoning	4.78028	0.07934	0.31703	0.00467	1775.2 ± 22.87	1790 ± 25.11
SPOT15	Zoning	4.33506	0.07692	0.30727	0.0047	1727.3 ± 23.19	1666.9 ± 27.51
SPOT17	Core	2.12318	0.04296	0.19487	0.00304	1147.7 ± 16.42	1173 ± 35.49
SPOT18	Zoning	4.25724	0.06603	0.29725	0.00441	1677.7 ± 21.91	1695.1 ± 21.38
SPOT19	Zoned Core	4.69604	0.0762	0.31806	0.00469	1780.3 ± 22.95	1752.7 ± 23.98
SPOT20	Zoned Core	4.08046	0.0714	0.29695	0.00448	1676.2 ± 22.25	1620.4 ± 27.57
SPOT21	Zoning	4.47145	0.0721	0.31011	0.00482	1741.2 ± 23.7	1706.6 ± 21.42
SPOT22	Structureless	4.528	0.07269	0.30755	0.00463	1728.6 ± 22.82	1745 ± 22.07
SPOT23	Zoned Core	4.06212	0.07002	0.27737	0.00409	1578.1 ± 20.66	1737.1 ± 27.02
SPOT25	Core	4.09748	0.06756	0.28712	0.00459	1627.1 ± 23	1687.1 ± 21.98
SPOT26	Structureless	5.06287	0.08173	0.32559	0.00501	1817 ± 24.38	1844.3 ± 21.65
SPOT27	Core	4.84804	0.07997	0.30736	0.00465	1727.7 ± 22.93	1870.1 ± 23.15
SPOT28	Core	4.42737	0.07462	0.30143	0.00484	1698.4 ± 23.96	1740 ± 22.79
SPOT29	Zoned Core	4.88662	0.07492	0.31867	0.00485	1783.2 ± 23.7	1818.8 ± 19.12
SPOT30	Structureless	4.56902	0.06772	0.30763	0.00451	1729.1 ± 22.21	1761.7 ± 19.29
SPOT31	Zoning	4.80192	0.07878	0.3215	0.00485	1797.1 ± 23.66	1772.4 ± 23.2
SPOT32	Possible Core	4.76489	0.08342	0.31651	0.00487	1772.7 ± 23.86	1787 ± 26.01
SPOT34	Zoned Core	3.79554	0.06027	0.27108	0.00405	1546.3 ± 20.52	1654 ± 22.01
SPOT35	Core	4.08222	0.07475	0.29087	0.00453	1645.9 ± 22.61	1658.5 ± 28.37
SPOT36	Zoning	4.93395	0.08828	0.33005	0.00512	1838.6 ± 24.82	1774.6 ± 26.98
SPOT37	Structureless	4.6658	0.07548	0.31289	0.0047	1754.9 ± 23.09	1770.2 ± 22.53
SPOT38	Zoning	3.08958	0.0464	0.25117	0.00361	1444.5 ± 18.6	1408.9 ± 21.58
SPOT39	Zoning	5.08887	0.08076	0.32447	0.00484	1811.5 ± 23.56	1860 ± 21.98
SPOT41	Core	4.26731	0.06928	0.28834	0.00429	1633.2 ± 21.46	1754.6 ± 23.03
SPOT42	Rim	4.7499	0.07188	0.31793	0.00456	1779.6 ± 22.31	1772 ± 21.2
SPOT43	Core	4.81156	0.07942	0.31505	0.00472	1765.5 ± 23.14	1812.1 ± 23.75
SPOT45	Zoning	4.07426	0.06775	0.2886	0.00433	1634.5 ± 21.66	1668.2 ± 24.6
SPOT47	Zoned Core	4.64055	0.06885	0.31246	0.00455	1752.8 ± 22.34	1761.4 ± 19.49
SPOT50	Core	3.94821	0.06527	0.28005	0.00435	1591.6 ± 21.9	1665.5 ± 23.35
SPOT51B	Zoning	4.03862	0.06442	0.28967	0.00423	1639.9 ± 21.12	1645.1 ± 23.75
SPOT52C	Zoning	3.93418	0.06069	0.28636	0.00417	1623.3 ± 20.89	1617.6 ± 22.13
SPOT53B	Core	4.7031	0.07353	0.31485	0.00464	1764.5 ± 22.74	1771.7 ± 22.19
SPOT54C	Zoning	4.57918	0.07124	0.31168	0.00465	1749 ± 22.85	1741.7 ± 21.31
SPOT55B	Zoning	4.04219	0.06261	0.28471	0.00409	1615 ± 20.54	1678.1 ± 22.85

SPOT56C	Zoning	4.04181	0.06158	0.2892	0.00418	1637.5 ± 20.91	1649.1 ± 21/78
SPOT57B	Core	4.72198	0.08497	0.31254	0.00497	1753.2 ± 24.42	1793.5 ± 26.9
SPOT58C	Core	4.53327	0.07665	0.3017	0.00463	1699.7 ± 22.95	1782.6 ± 24.73
SPOT59B	Core	4.25239	0.06285	0.29731	0.00441	1678 ± 21.9	1691.8 ± 19.17
SPOT61B	Structureless	4.36181	0.06904	0.29728	0.00439	1677.8 ± 21.82	1738.7 ± 22.8
SPOT62B	Zoning	3.98469	0.06356	0.28609	0.00436	1622 ± 21.88	1643.2 ± 22.1
SPOT63B	Zoning	4.00764	0.06206	0.28764	0.00427	1629.7 ± 21.38	1643.6 ± 21.63
SPOT64C	Zoning	4.13116	0.06638	0.29037	0.00424	1643.4 ± 21.18	1682.2 ± 24.15
SPOT65B	Core	5.11784	0.0782	0.32381	0.00469	1808.3 ± 22.84	1874.4 ± 21.47
SPOT66B	Core (lead depletion evident)	2.15807	0.04158	0.19374	0.00307	1141.6 ± 16.58	1216.7 ± 31.94
SPOT67B	Zoned Core	4.71152	0.07222	0.31423	0.00467	1761.5 ± 22.92	1778.7 ± 20.53
SPOT68B	Zoning	3.19128	0.05028	0.25444	0.00397	1461.3 ± 20.4	1447.4 ± 20.97
SPOT69B	Zoned Core	4.51846	0.07084	0.30587	0.00468	1720.4 ± 23.11	1751.9 ± 20.36
SPOT70B	Zoning	3.5107	0.06199	0.26713	0.004	1526.2 ± 20.33	1534.1 ± 28.36

SHRIMP analyses used for constraining the timing of deformation

Sample ORM7

Incremental Heating			36Ar(a)	37Ar(ca)	38Ar(cl)	39Ar(k)	40Ar(r)	Age (Ma)	± 2s	40Ar(r) (%)	39Ar(k) (%)	K/Ca	± 2s
9A6936D	55.80 W		0.000021	0.000000	0.000001	0.000002	0.000000	0.00	± 0.00	0.00	0.00		
9A6939D	56.30 W		0.000062	0.000371	0.000000	0.027548	0.664243	352.46	± 4.98	97.33	28.89	31.912	± 51.151
9A6940D	56.40 W		0.000021	0.000000	0.000002	0.003763	0.084797	331.39	± 17.91	93.17	3.95	43.439	± 78.335
9A6941D	56.50 W		0.000041	0.000000	0.000000	0.011345	0.264408	341.72	± 9.83	95.59	11.90	43.439	± 78.335
9A6942D	56.60 W		0.000022	0.000000	0.000000	0.005134	0.117692	336.59	± 18.91	94.74	5.38	43.439	± 78.335
9A6944D	56.70 W		0.000025	0.000000	0.000000	0.010484	0.249493	348.26	± 9.34	97.09	10.99	43.439	± 78.335
9A6945D	56.80 W		0.000002	0.000025	0.000004	0.003486	0.082350	345.92	± 20.17	99.45	3.66	59.036	± 1483.923
9A6957D	57.00 W		0.000000	0.000000	0.000000	0.006901	0.165775	351.26	± 6.21	100.00	7.24	8.065	± 23.897
9A6958D	57.20 W		0.000000	0.000000	0.000013	0.005075	0.120118	346.53	± 7.31	100.00	5.32	8.065	± 23.897
9A6959D	57.40 W		0.000000	0.000000	0.000011	0.011993	0.289233	352.51	± 3.64	100.00	12.58	8.065	± 23.897
9A6960D	57.70 W		0.000012	0.000000	0.000007	0.001920	0.043707	334.42	± 59.20	92.69	2.01	8.065	± 23.897
9A6962D	58.00 W		0.000000	0.000000	0.000000	0.002836	0.067047	346.23	± 13.90	100.00	2.97	8.065	± 23.897
9A6963D	58.30 W		0.000000	0.000000	0.000002	0.004695	0.110234	344.05	± 4.16	100.00	4.92	8.065	± 23.897
9A6964D	61.00 W		0.000006	0.000000	0.000012	0.000185	0.013949	931.94	± 356.25	88.48	0.19	8.065	± 23.897
		S	0.000211	0.000397	0.000052	0.095368	2.273048						

Table 5a)

Statistics

Information on Analysis		Results	40(r)/39(k)	± 2s	Age (Ma)	± 2s	MSWD	39Ar(k) (%,n)	K/Ca	± 2s
ORM-7		**Weighted Plateau**	23.9344	± 0.2013	350.09	± 2.69	1.41	94.88	11.354	± 10.107
Ser				± 0.84%		± 0.77%		11		
Laser					External Error	± 2.97	2.23	Statistical T Ratio		
CJL					Analytical Error	± 2.68	1.1855	Error Magnification		
Project = ArabiaCJL		**Total Fusion Age**	23.8345	± 0.2332	348.76	± 3.11		14	103.404	± 547.715
Irradiation = I5t25h				± 0.98%		± 0.89%				
J = 0.0089480 ± 0.0000					External Error	± 3.36				
FCs = 28.030 ± 0.078 M					Analytical Error	± 3.10				

Table 5b)

Sample ORM8

Incremental Heating			36Ar(a)	37Ar(ca)	38Ar(cl)	39Ar(k)	40Ar(r)	Age (Ma)	± 2s	40Ar(r) (%)	39Ar(k) (%)	K/Ca	± 2s
9A6965D	56.20 W		0.000041	0.000000	0.000006	0.000014	0.030437	5420.17	± 3059.79	71.42	0.02		
9A6967D	56.50 W		0.000017	0.000000	0.000003	0.000059	0.010430	1715.42	± 842.49	67.02	0.08		
9A6968D	56.80 W		0.000035	0.000000	0.000002	0.000183	0.060970	2492.35	± 204.29	85.58	0.25	1.239	± 6.022
9A6969D	57.10 W		0.000158	0.000128	0.000012	0.001387	0.127001	1079.46	± 54.84	73.15	1.87	4.647	± 51.573
9A6970D	57.40 W		0.000025	0.000250	0.000000	0.006286	0.193227	438.35	± 13.32	96.25	8.49	10.804	± 61.330
9A6972D	57.80 W		0.000000	0.000000	0.000006	0.004725	0.126912	388.54	± 8.24	100.00	6.38	7.395	± 8.320
9A6973D	58.30 W		0.000000	0.000000	0.000000	0.011663	0.331148	408.42	± 6.05	100.00	15.75	7.395	± 8.320
9A6974D	58.60 W		0.000000	0.000420	0.000000	0.005471	0.145909	386.11	± 6.80	100.00	7.39	5.598	± 18.833
9A6975D	59.00 W		0.000003	0.000205	0.000000	0.008184	0.217049	384.15	± 13.83	99.57	11.05	17.131	± 119.575
9A6976D	59.30 W		0.000000	0.000684	0.000000	0.003911	0.101660	377.22	± 5.66	100.00	5.28	2.461	± 5.088
9A6980D	59.60 W		0.000000	0.000000	0.000000	0.004399	0.114762	378.49	± 5.97	100.00	5.94	2.461	± 5.088
9A6981D	60.00 W		0.000018	0.000000	0.000010	0.012733	0.364738	411.66	± 9.60	98.60	17.19	2.461	± 5.088
9A6983D	60.30 W		0.000000	0.000000	0.000000	0.002454	0.073939	430.57	± 9.26	100.00	3.31	2.461	± 5.088
9A6984D	61.00 W		0.000007	0.000000	0.000000	0.003903	0.118797	434.59	± 22.33	98.20	5.27	2.461	± 5.088
9A6985D	61.70 W		0.000006	0.000000	0.000000	0.005745	0.190318	468.39	± 15.46	99.04	7.76	2.461	± 5.088
9A6986D	63.00 W		0.000003	0.000007	0.000000	0.001877	0.072990	538.64	± 39.75	98.73	2.53	111.466	± 5976.710
9A6990D	70.00 W		0.000134	0.000000	0.000004	0.001061	0.161358	1549.33	± 42.37	80.28	1.43	111.466	± 5976.710
		S	0.000448	0.001695	0.000043	0.074057	2.441647						

Table 6a)

Statistics

Information on Analysis		Results	40(r)/39(k)	± 2s	Age (Ma)	± 2s	MSWD	39Ar(k) (%,n)	K/Ca	± 2s
ORM-8		**Maximum age**	26.2236	± 0.3286	380	± 4.30	1.59	29.66	2.584	± 3.532
Ser				± 1.25%		± 1.13%		4		
Laser					External Error	± 4.52	3.18	Statistical T Ratio		
CJL					Analytical Error	± 4.30	1.2611	Error Magnification		
Project = ArabiaCJL		**Total Fusion Age**	32.9698	± 0.3497	466.39	± 4.37		17	18.787	± 52.337
Irradiation = I5t25h				± 1.06%		± 0.94%				
J = 0.0089480 ± 0.00000					External Error	± 4.68				
FCs = 28.030 ± 0.078 M					Analytical Error	± 4.36				

Table 6b)

Figure 1. Regional Map – Ormiston Gorge and Mount Sonder section traces

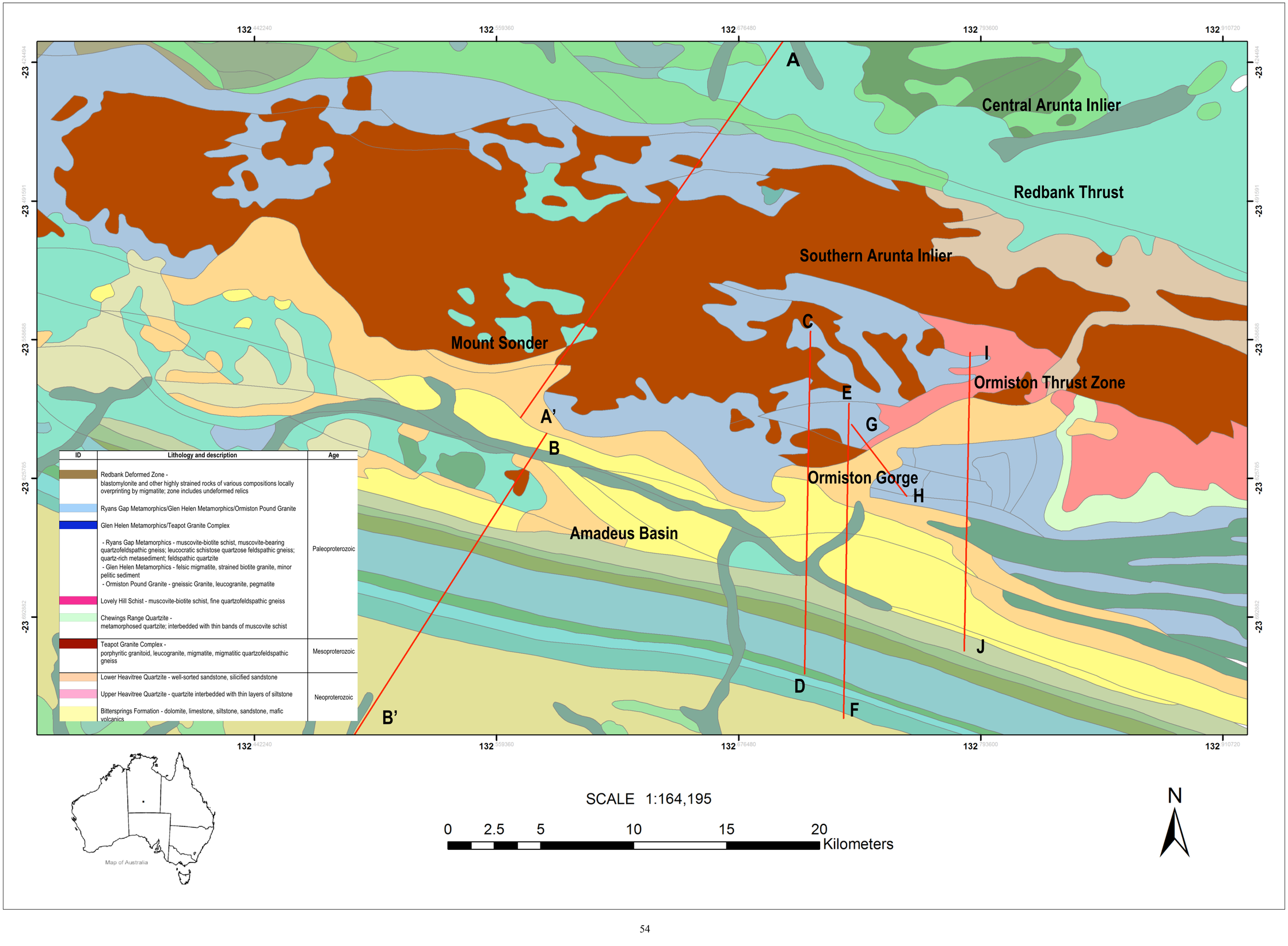

Figure 2. Ormiston Gorge Map

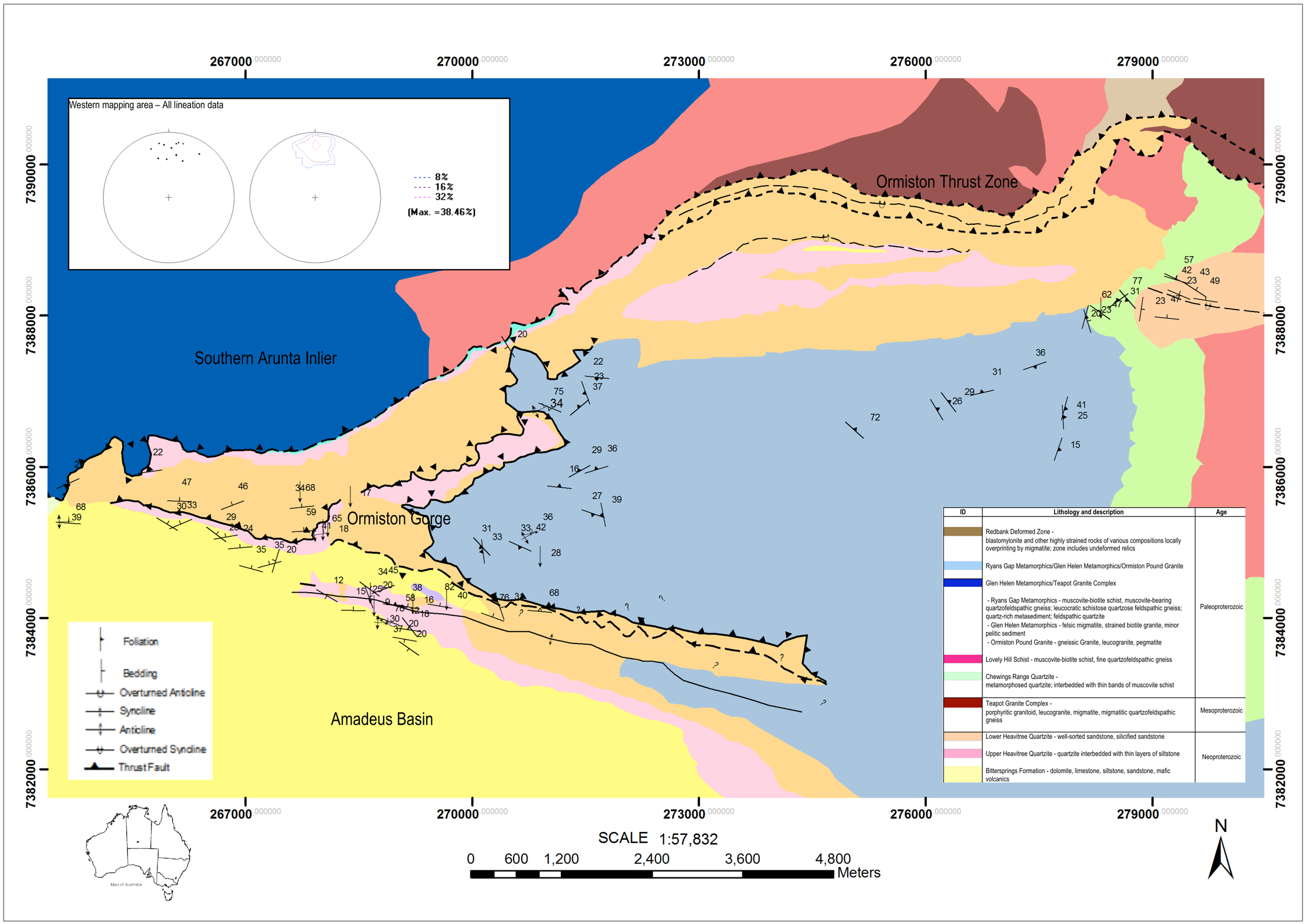

ID	Lithology and description	Age
	Redbank Deformed Zone - blastomylonite and other highly strained rocks of various compositions locally overprinting by migmatite; zone includes undeformed relics	Paleoproterozoic
	Ryans Gap Metamorphics/Glen Helen Metamorphics/Ormiston Pound Granite	
	Glen Helen Metamorphics/Teapot Granite Complex	
	- Ryans Gap Metamorphics - muscovite-biotite schist, muscovite-bearing quartzofeldspathic gneiss; leucocratic schistose quartzose feldspathic gneiss; quartz-rich metasediment; feldspathic quartzite - Glen Helen Metamorphics - felsic migmatite, strained biotite granite, minor pelitic sediment - Ormiston Pound Granite - gneissic Granite, leucogranite, pegmatite	
	Lovely Hill Schist - muscovite-biotite schist, fine quartzofeldspathic gneiss	
	Chewings Range Quartzite - metamorphosed quartzite; interbedded with thin bands of muscovite schist	
	Teapot Granite Complex - porphyritic granitoid, leucogranite, migmatite, migmatitic quartzofeldspathic gneiss	Mesoproterozoic
	Lower Heavitree Quartzite - well-sorted sandstone, silicified sandstone	Neoproterozoic
	Upper Heavitree Quartzite - quartzite interbedded with thin layers of siltstone	
	Bitterspring Formation - dolomite, limestone, siltstone, sandstone, mafic volcanics	

Figure 3. Ormiston Gorge – western mapping area

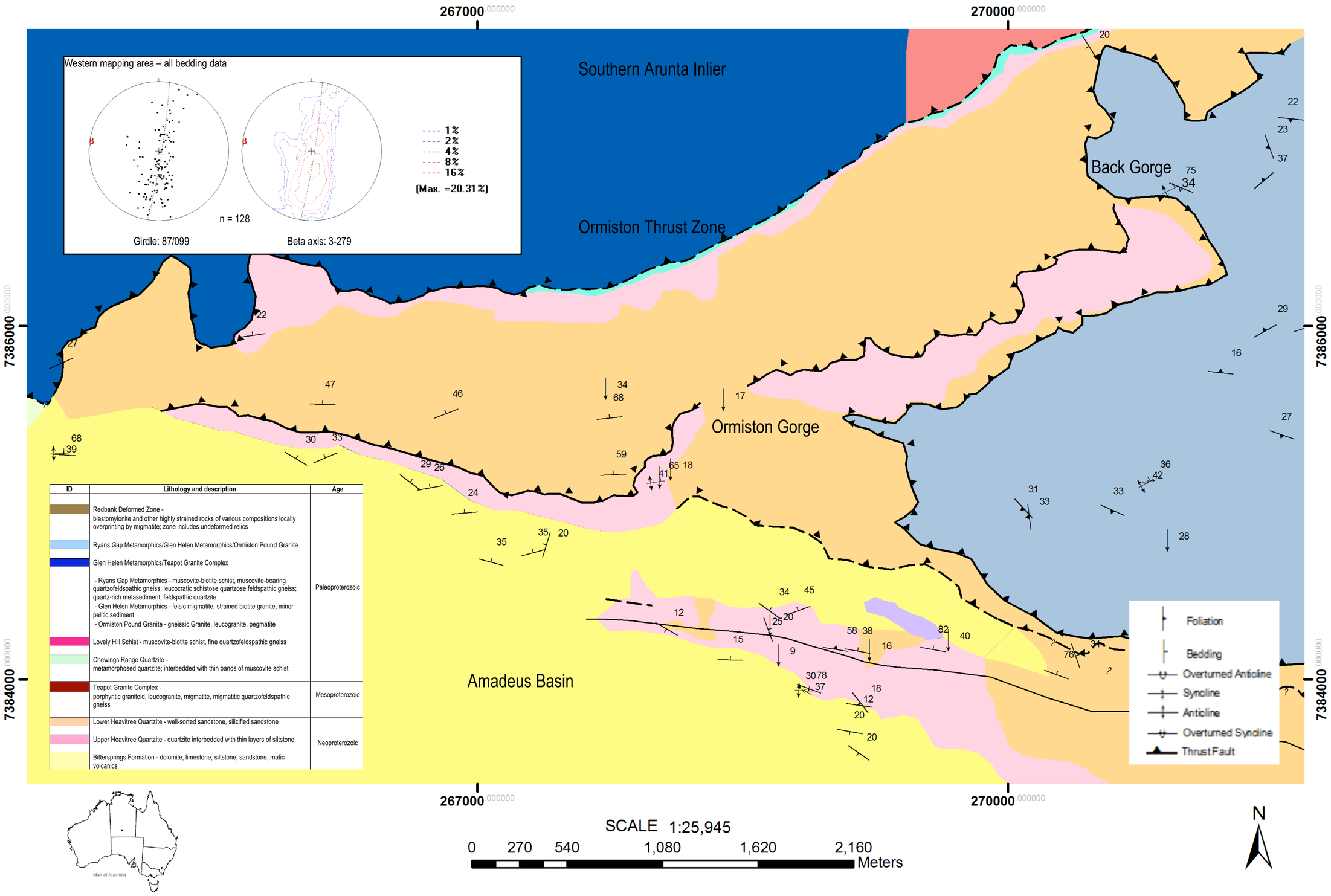

Figure 4. Ormiston Gorge – northeast mapping area

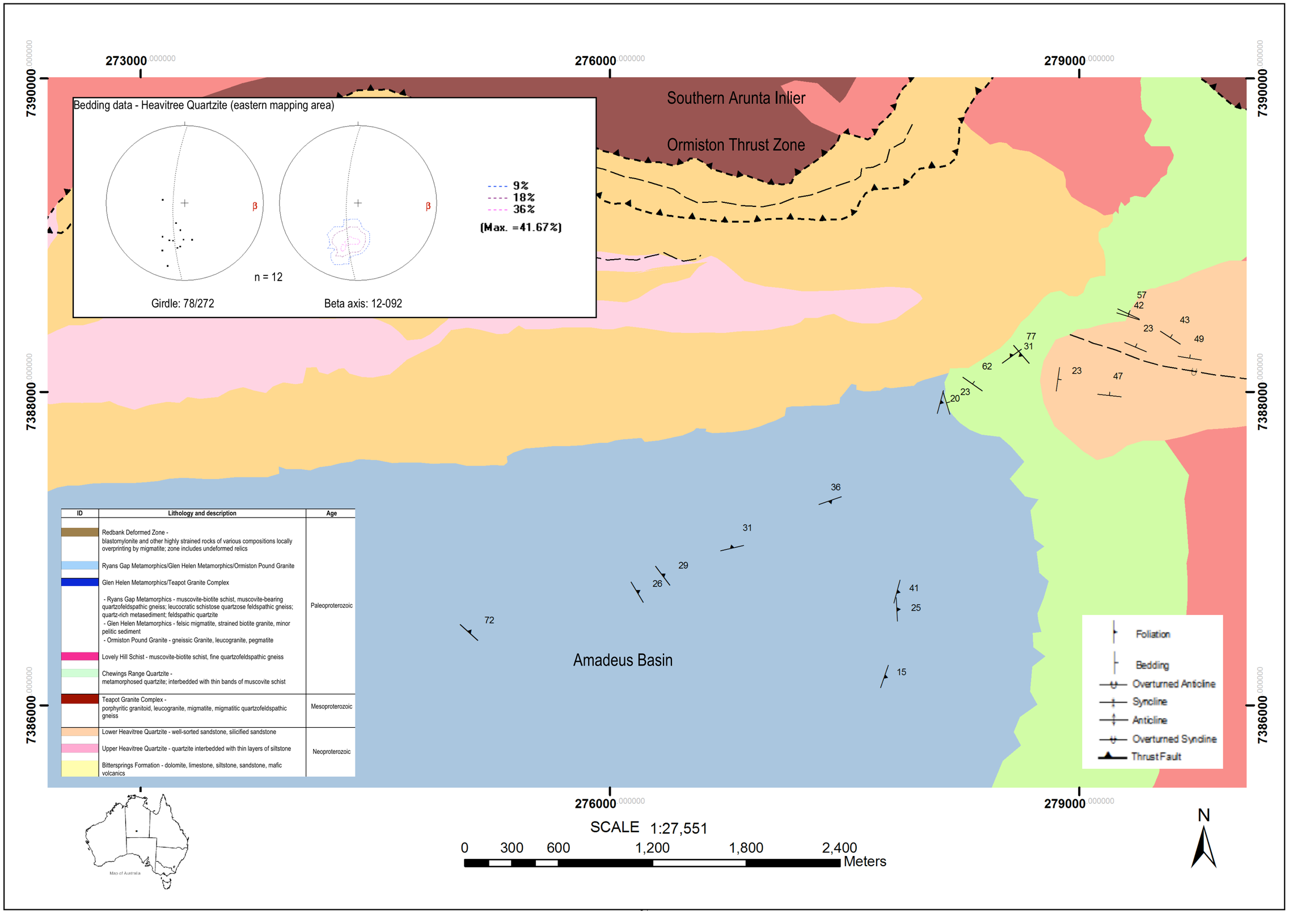

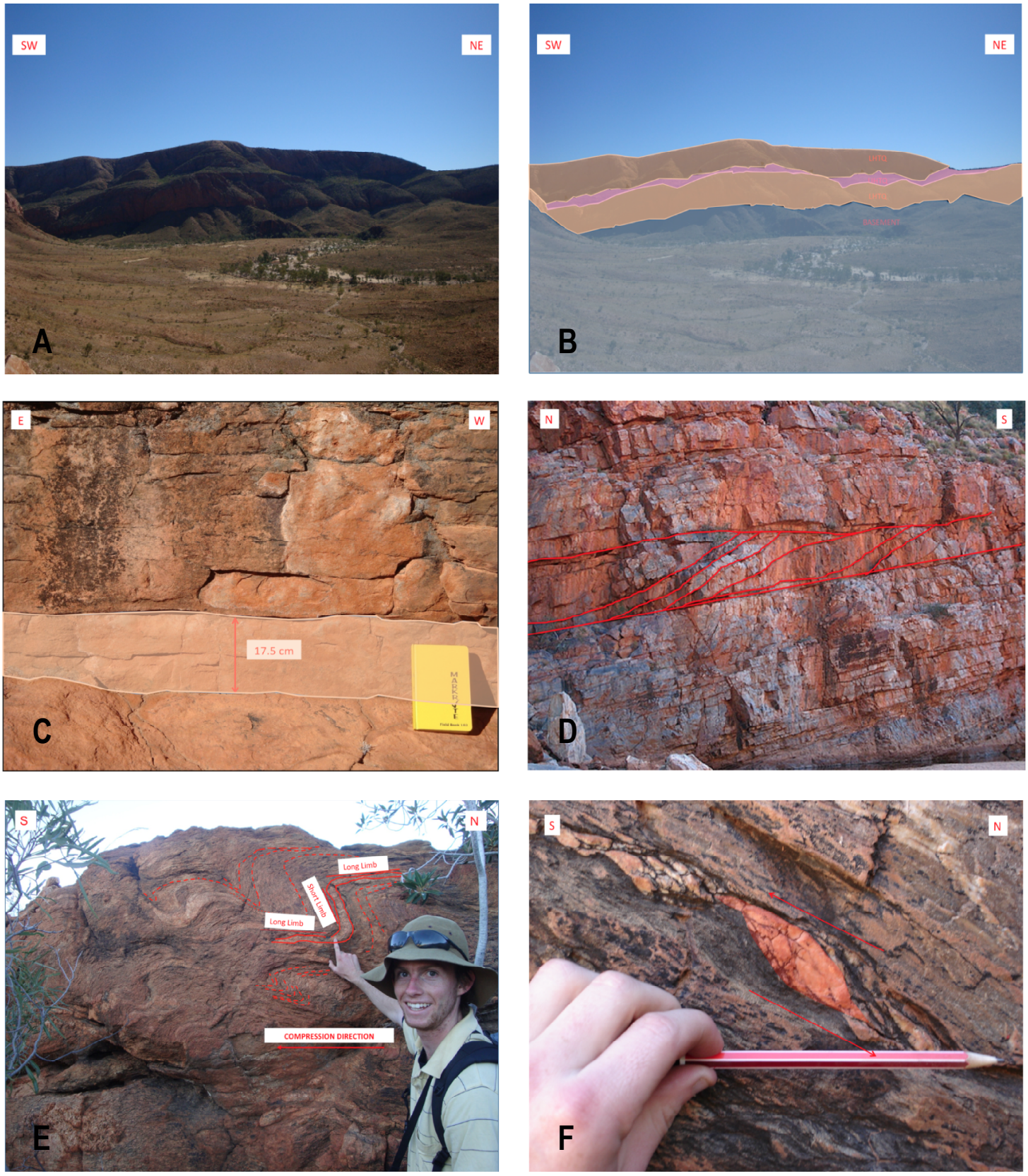
SW
NE
A
SW
NE
UHTQ
UHTQ
UHTQ
BASEMENT
B
E
W
17.5 cm
C
N
S
D
S
N
Long Limb
Short Limb
Long Limb
COMPRESSION DIRECTION
E
S
N
F

Figure 5

Figure 6 - Axial Plane

Western mapping area – All axial plane data

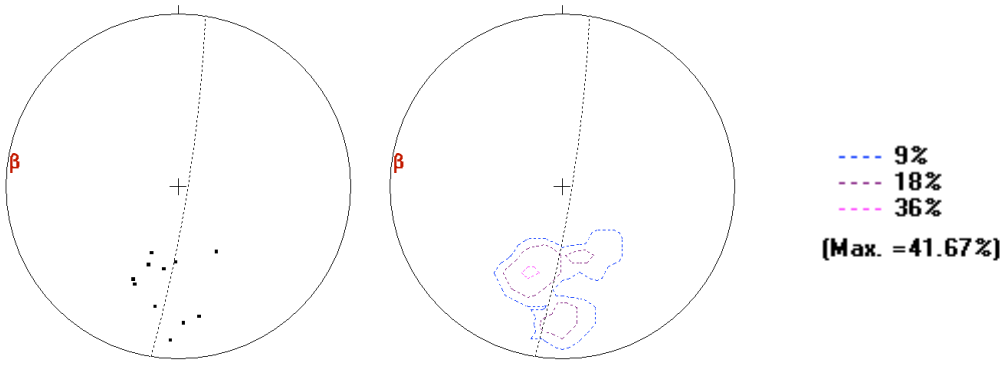

Girdle: 86/099 Beta axis: 4-279

Figure 7 - Lineation

Western mapping area – All lineation data

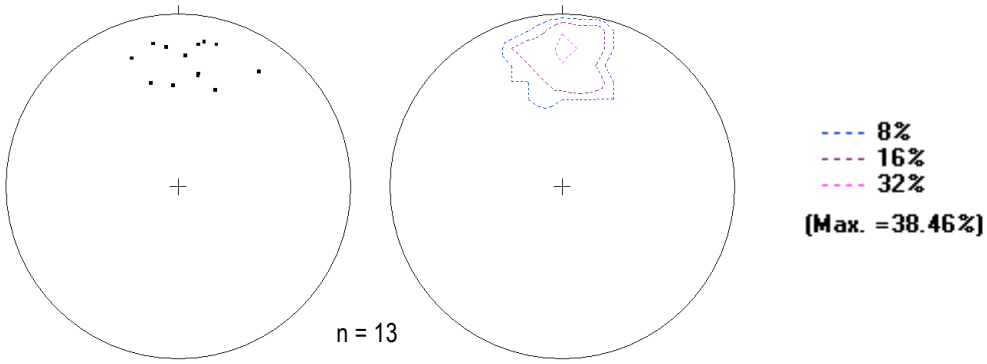

n = 13

Figure 8 - Foliation

Western and eastern mapping area – All foliation data

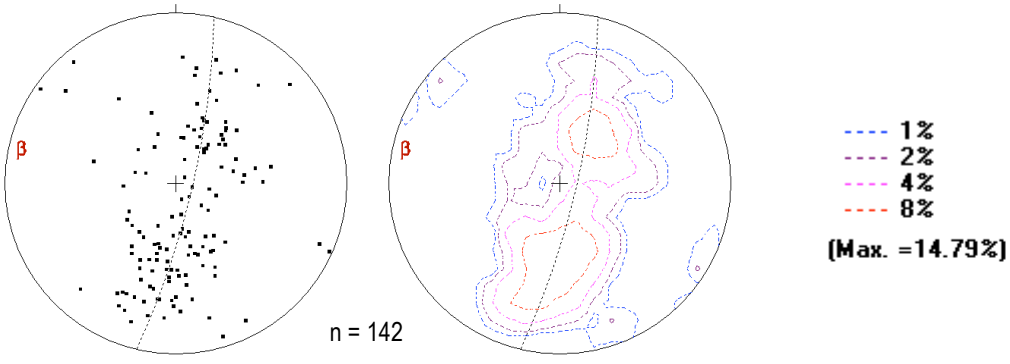

n = 142

Girdle: 82/103 Beta axis: 8-283

Figure 6, 7 and 8

Figure 9 - Bedding

9a) Western mapping area – all bedding data

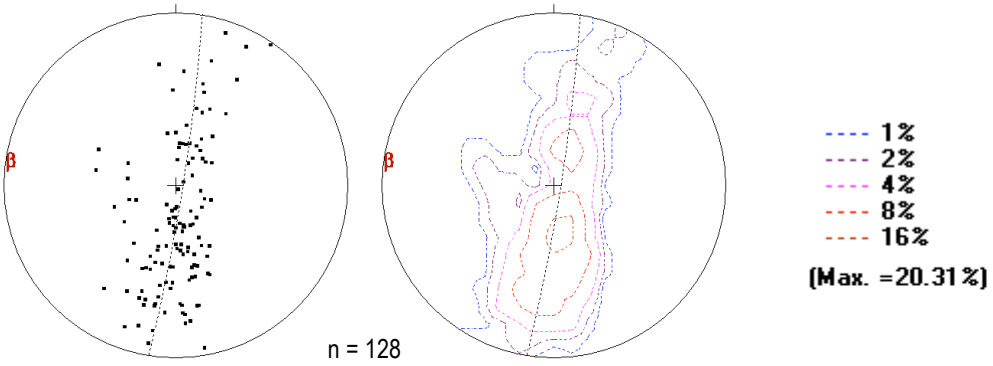

n = 128

Girdle: 87/099 Beta axis: 3-279

9b) Western mapping area – Lower Heavitree Quartzite

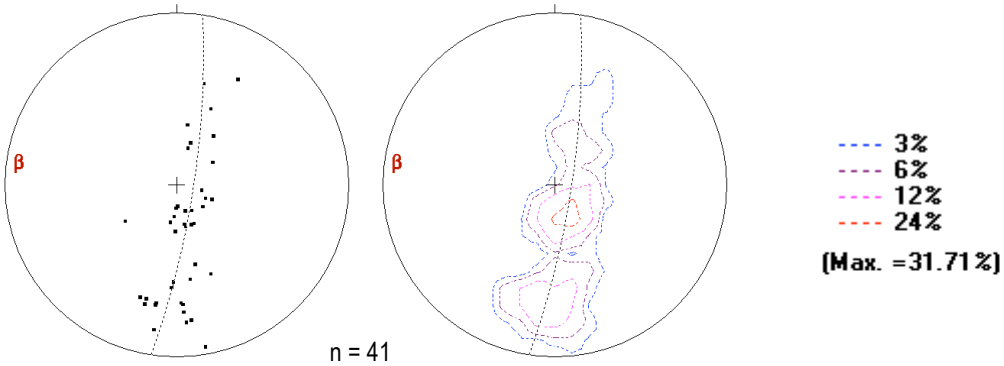

n = 41

Girdle: 82/099 Beta axis: 8-279

9c) Western mapping area – Upper Heavitree Quartzite

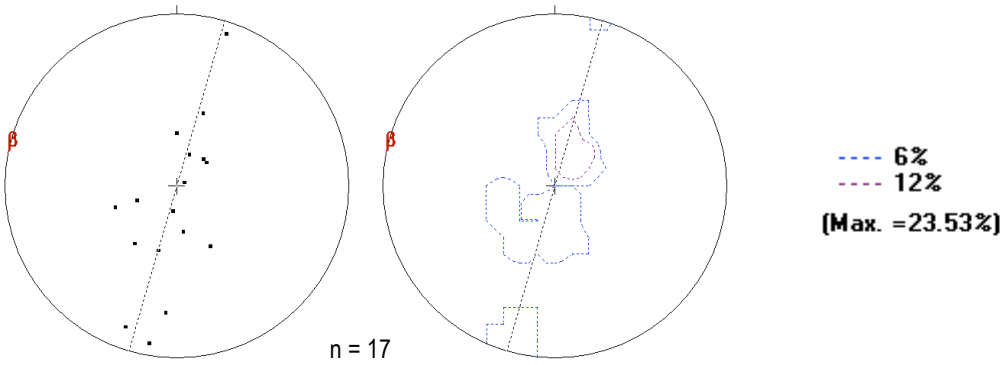

n = 17

Girdle: 89/106 Beta axis: 1-286

Figure 9

9d) Western mapping area – Bittersprings Formation

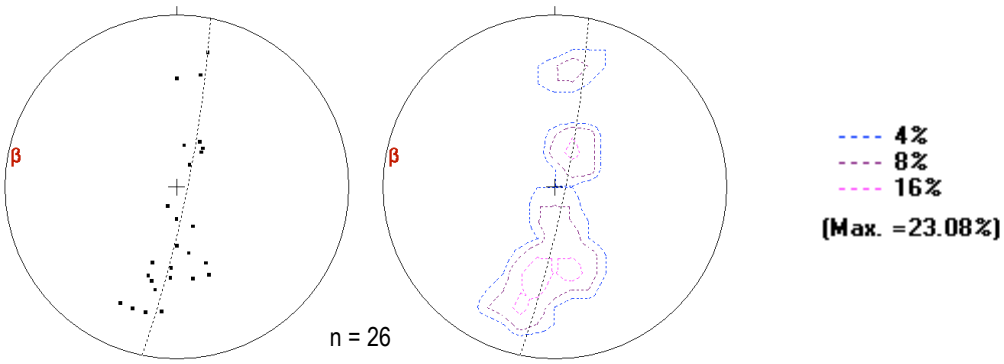

n = 26

Girdle: 85/102 Beta axis: 5-282

9e) Eastern mapping area - Heavitree Quartzite bedding data

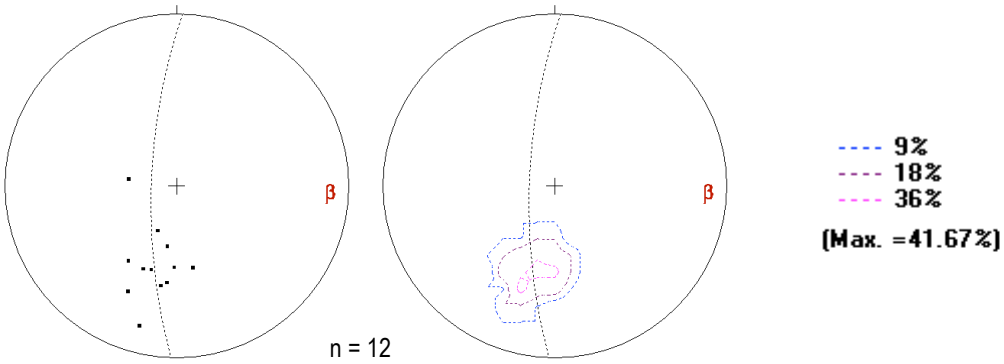

n = 12

Girdle: 78/272 Beta axis: 12-092

Figure 10 - Fold Hinge

Western mapping area – All fold hinge data

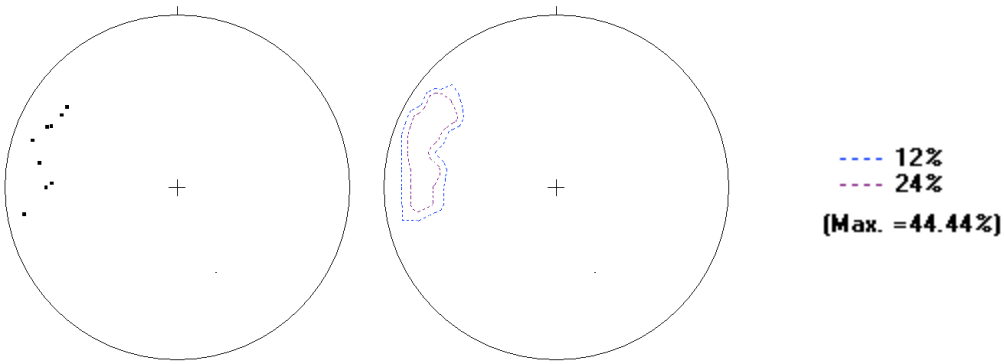

U-Pb dating of detrital zircons

Sample 40A_PQ - Pebble Quartzite

11a) Internal structure of the detrital zircons

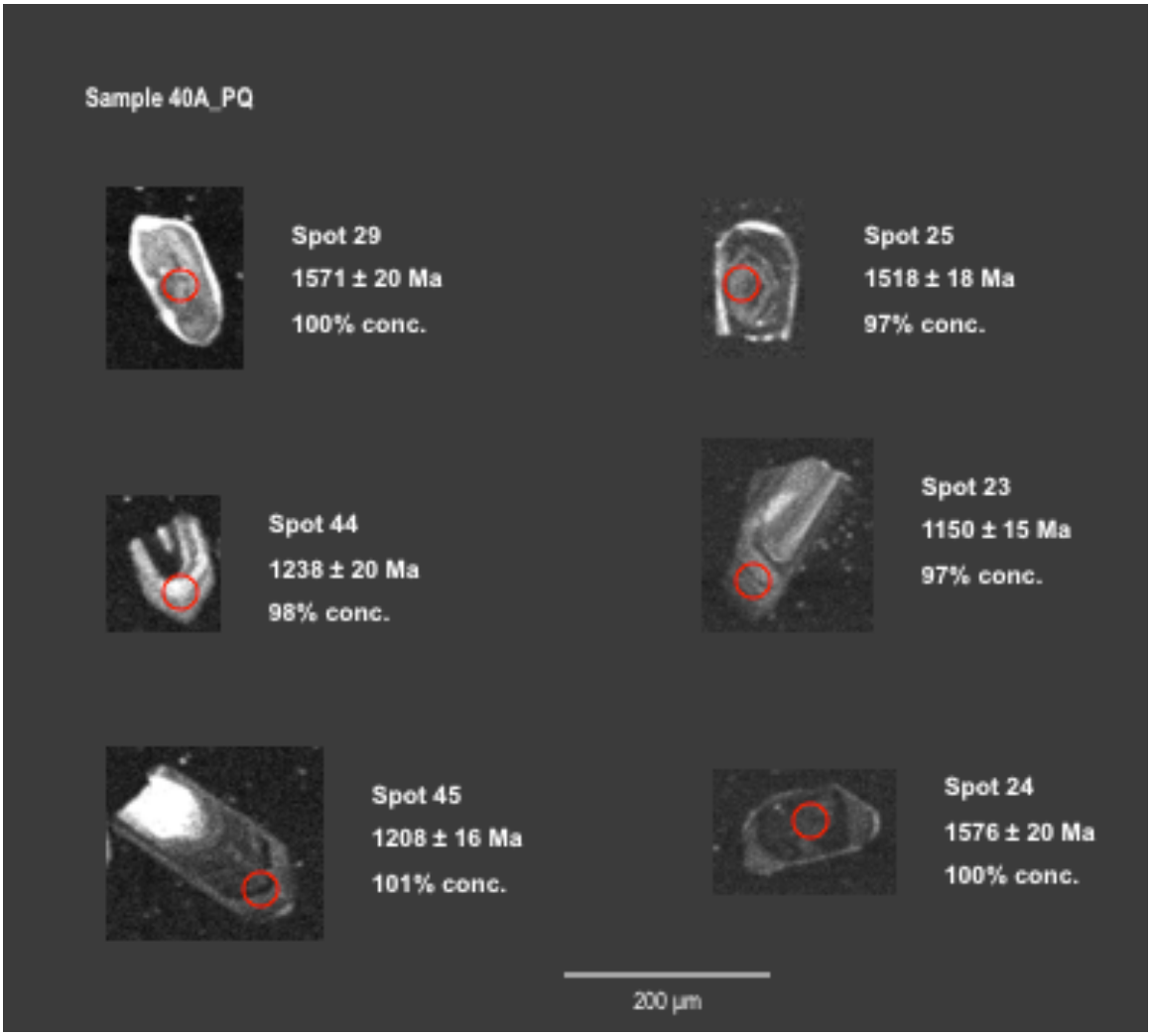

Figure 11

11b) All zircon age data

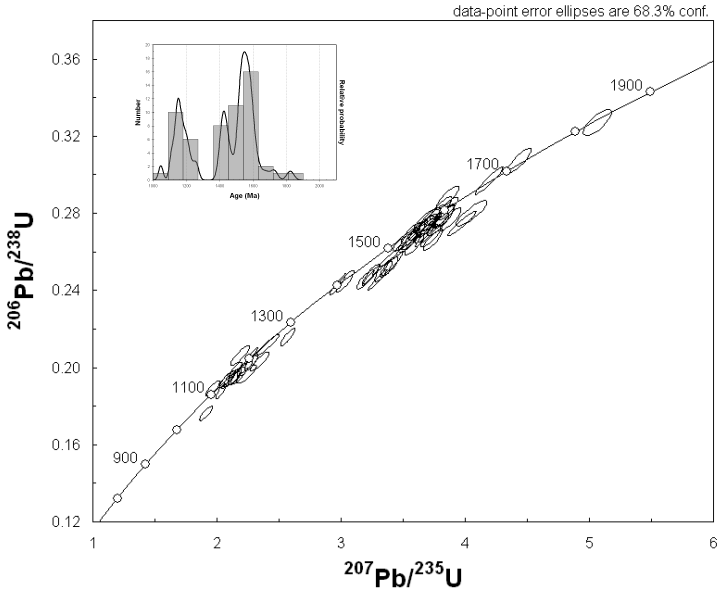

11c) Zircon core age data

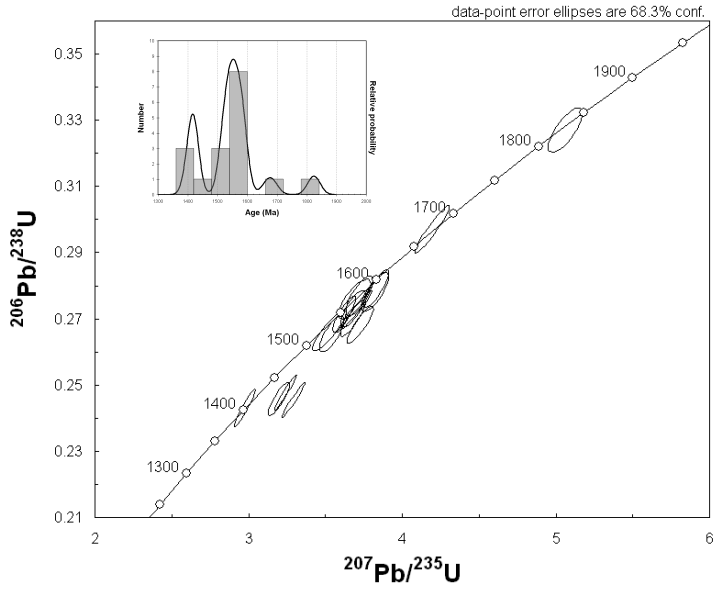

Figure 11 cont.

11d) Zircon rim age data

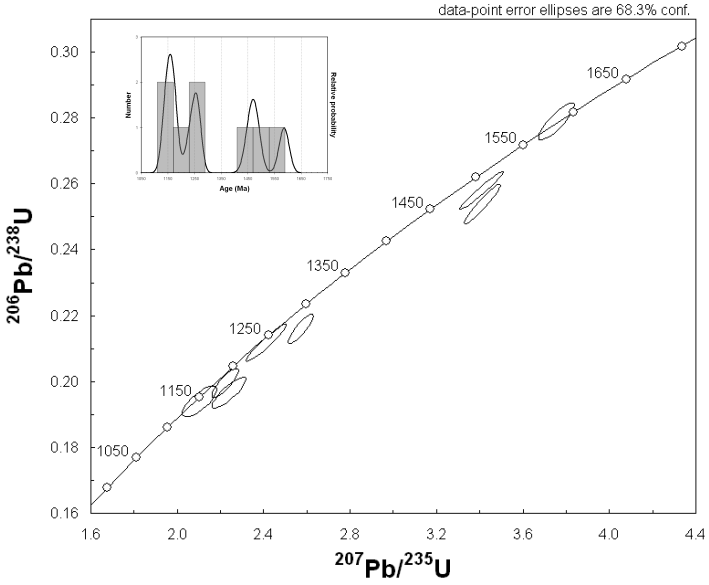

Figure 11 cont.

Sample 40C_LHTQ - Lower Heavitree Quartzite

12a) Internal structure of the detrital zircons

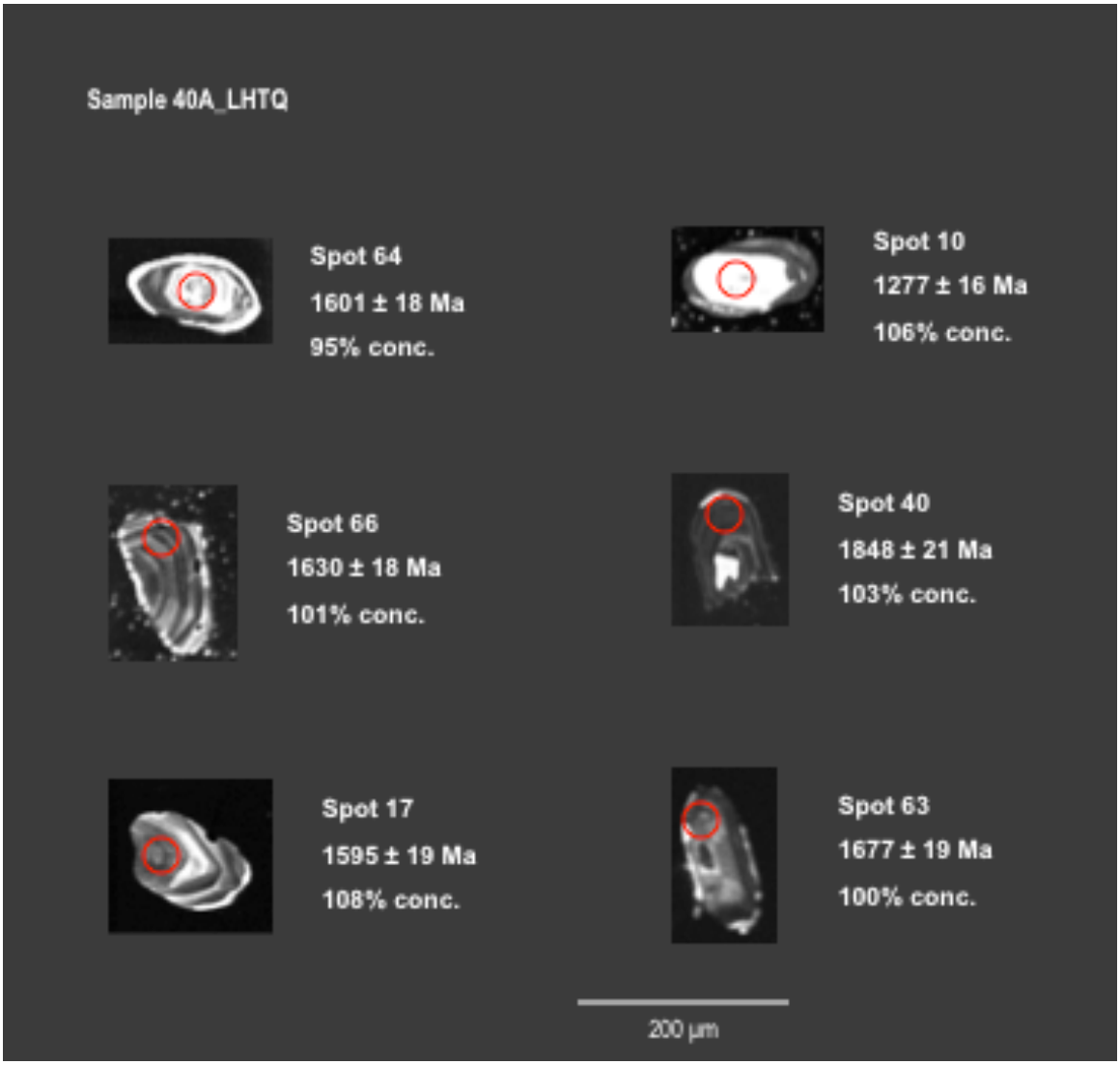

Figure 12

12b) All zircon age data

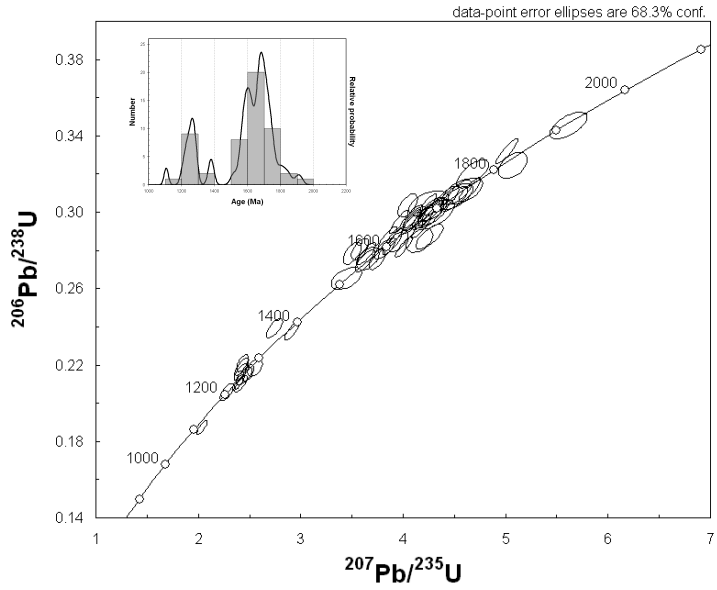

12c) Zircon core age data

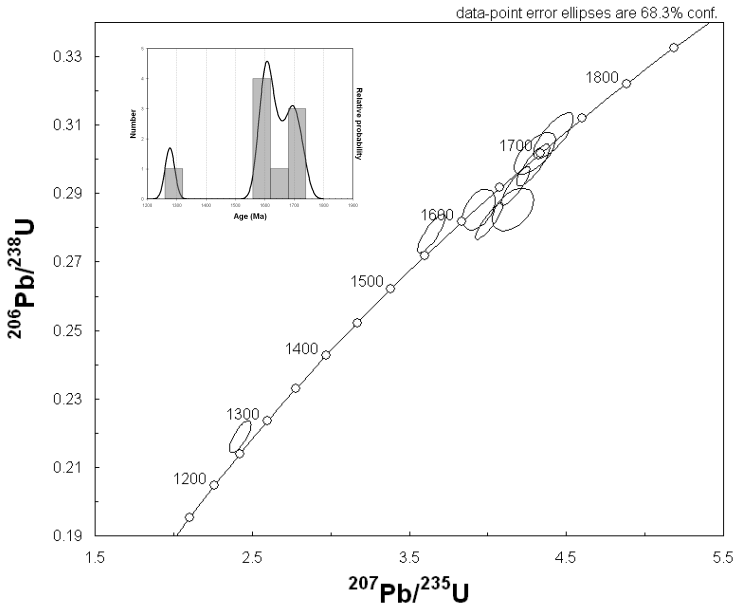

Figure 12 cont.

12d) Zircon rim age data

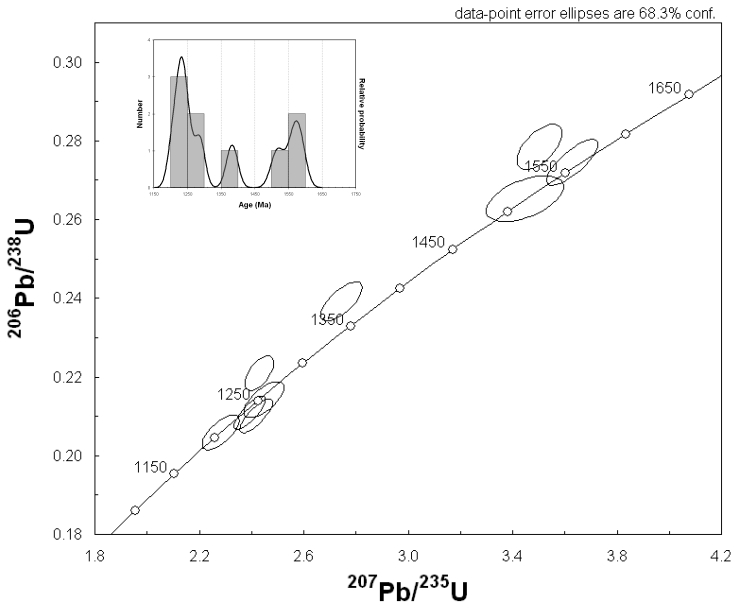

Figure 12 cont.

Sample 34B_CQ - Chewings Range Quartzite

13a) Internal structure of the detrital zircons

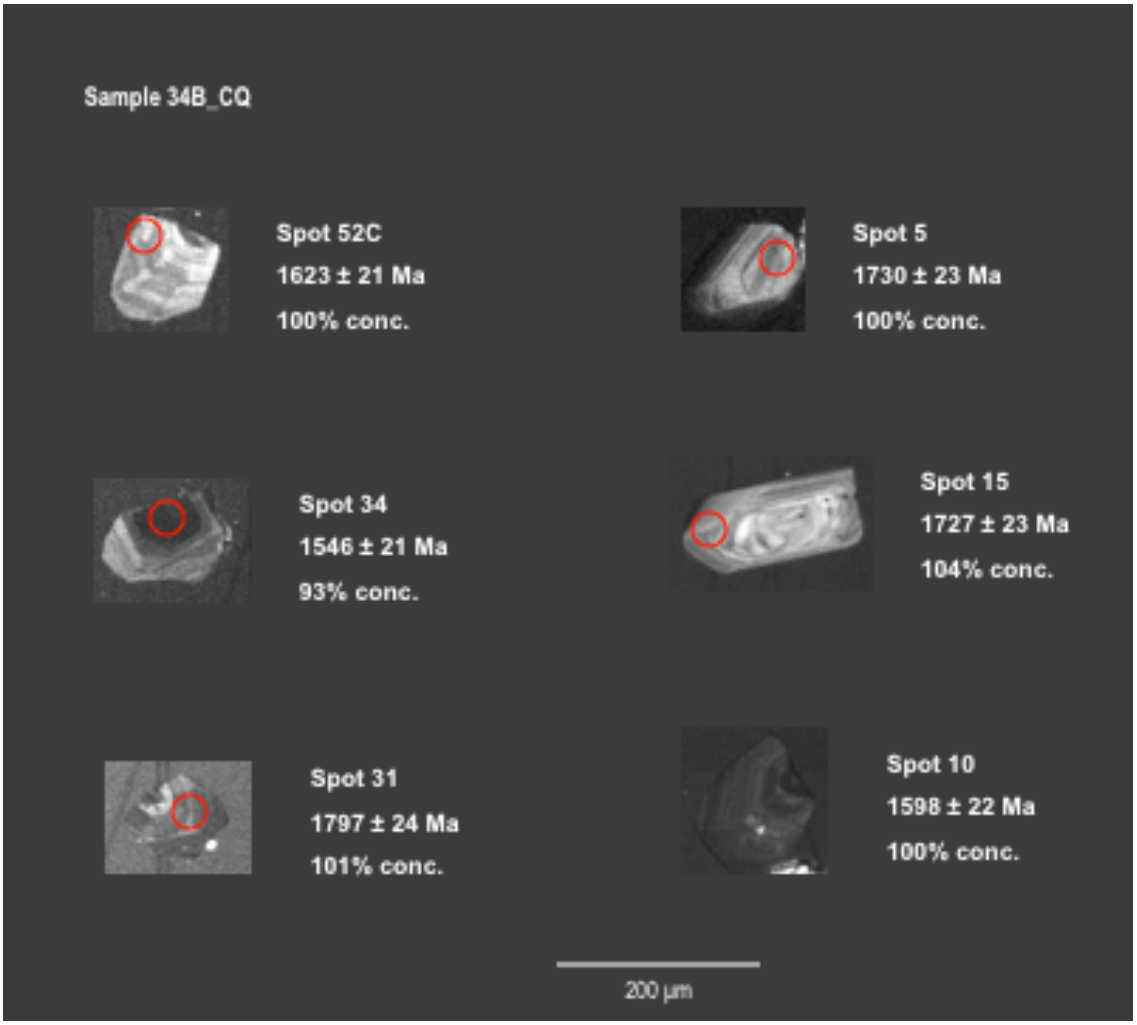

Figure 13

13b) All zircon age data

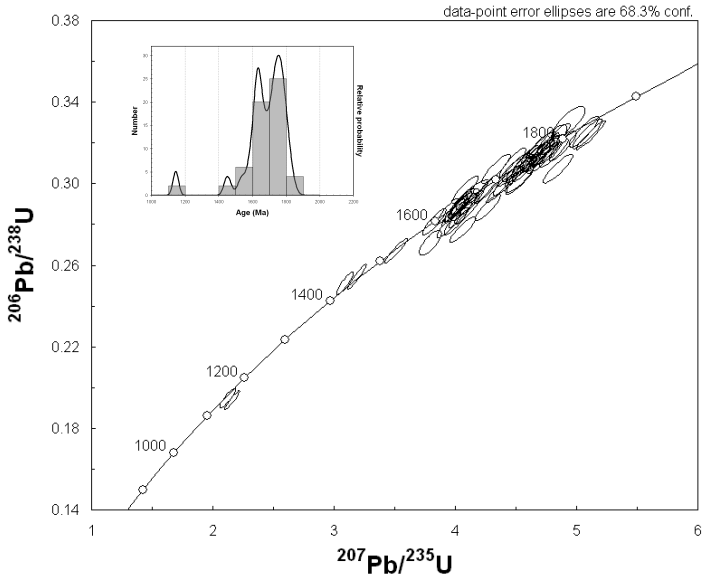

13c) Zircon core age data

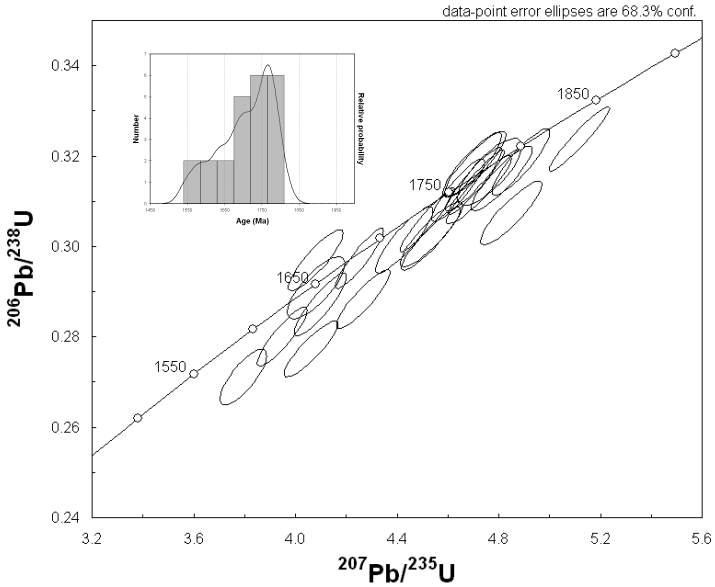

Figure 13 cont.

$^{40}Ar/^{39}Ar$ dating of muscovite

Sample ORM7

14a) Age Plateau

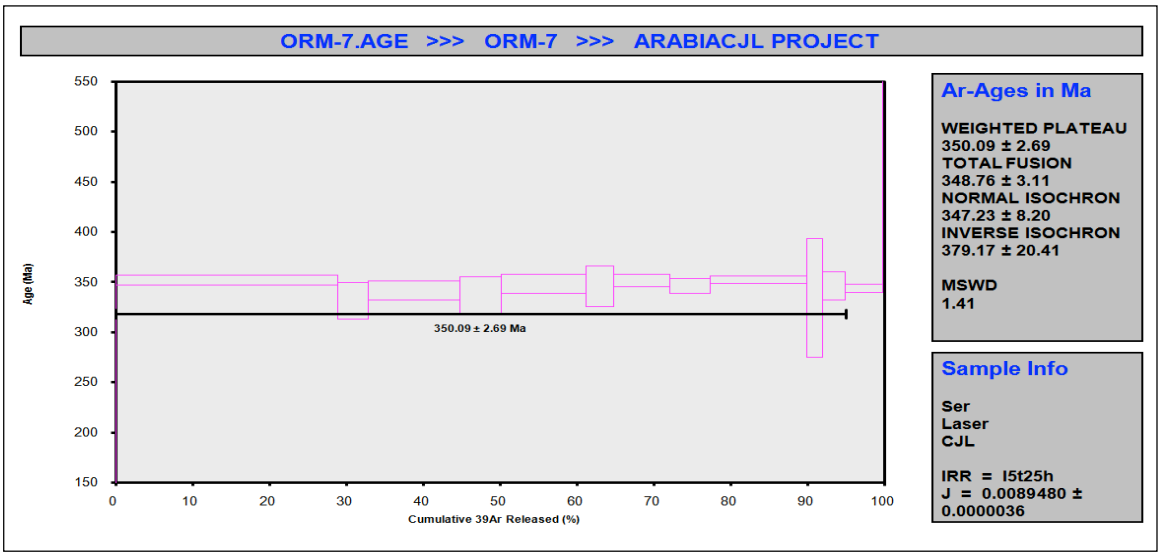

14b) Normal Isochron

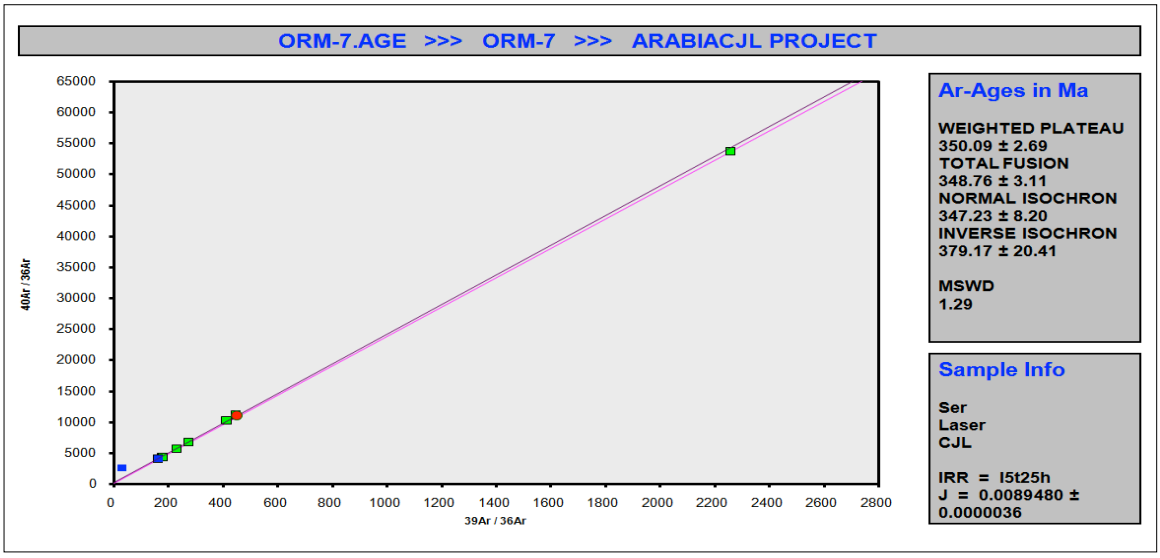

Figure 14

Sample ORM8

15a) Age Plateau

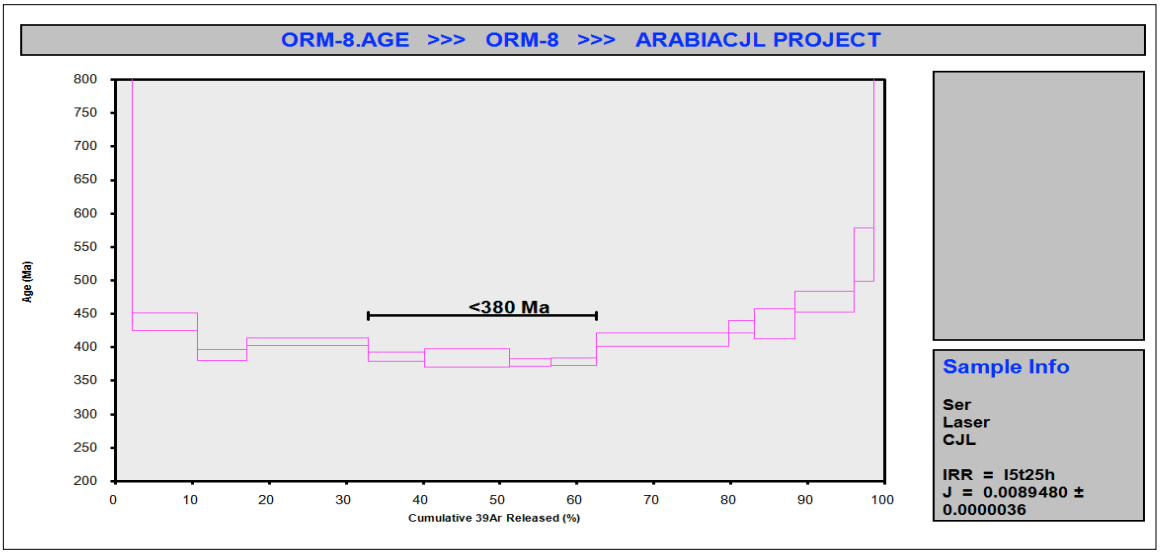

15b) Normal Isochron

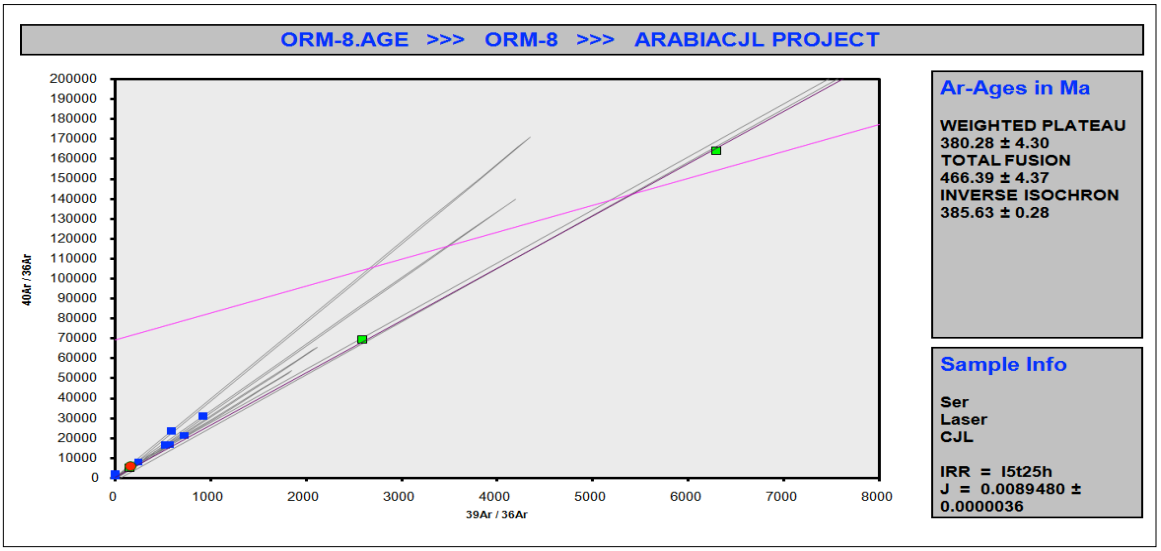

Figure 15

Mount Sonder section trace (Flottmann & Hand, 1999)

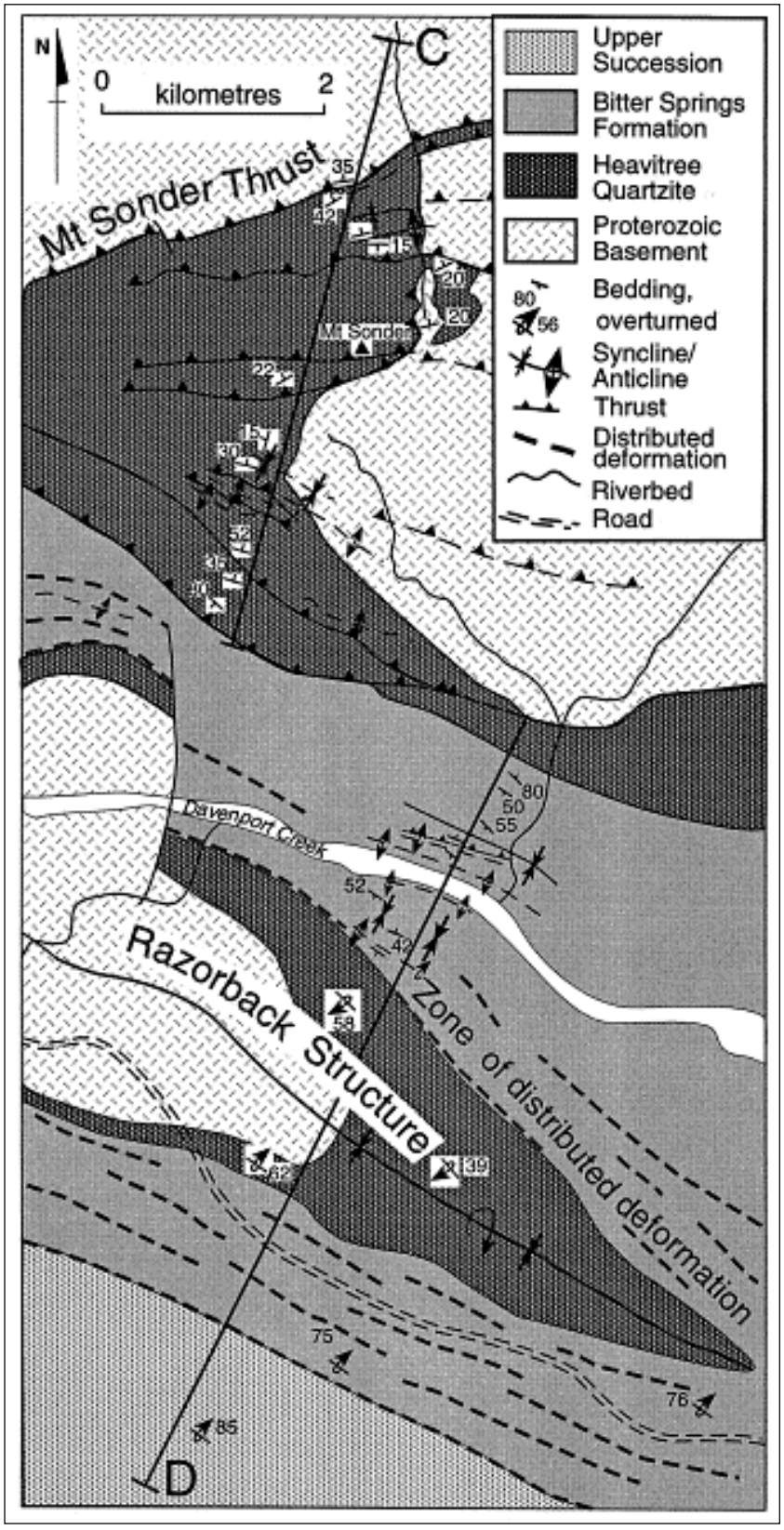

Figure 16

Mount Sonder cross-section – restored section (Flottmann & Hand, 1999)

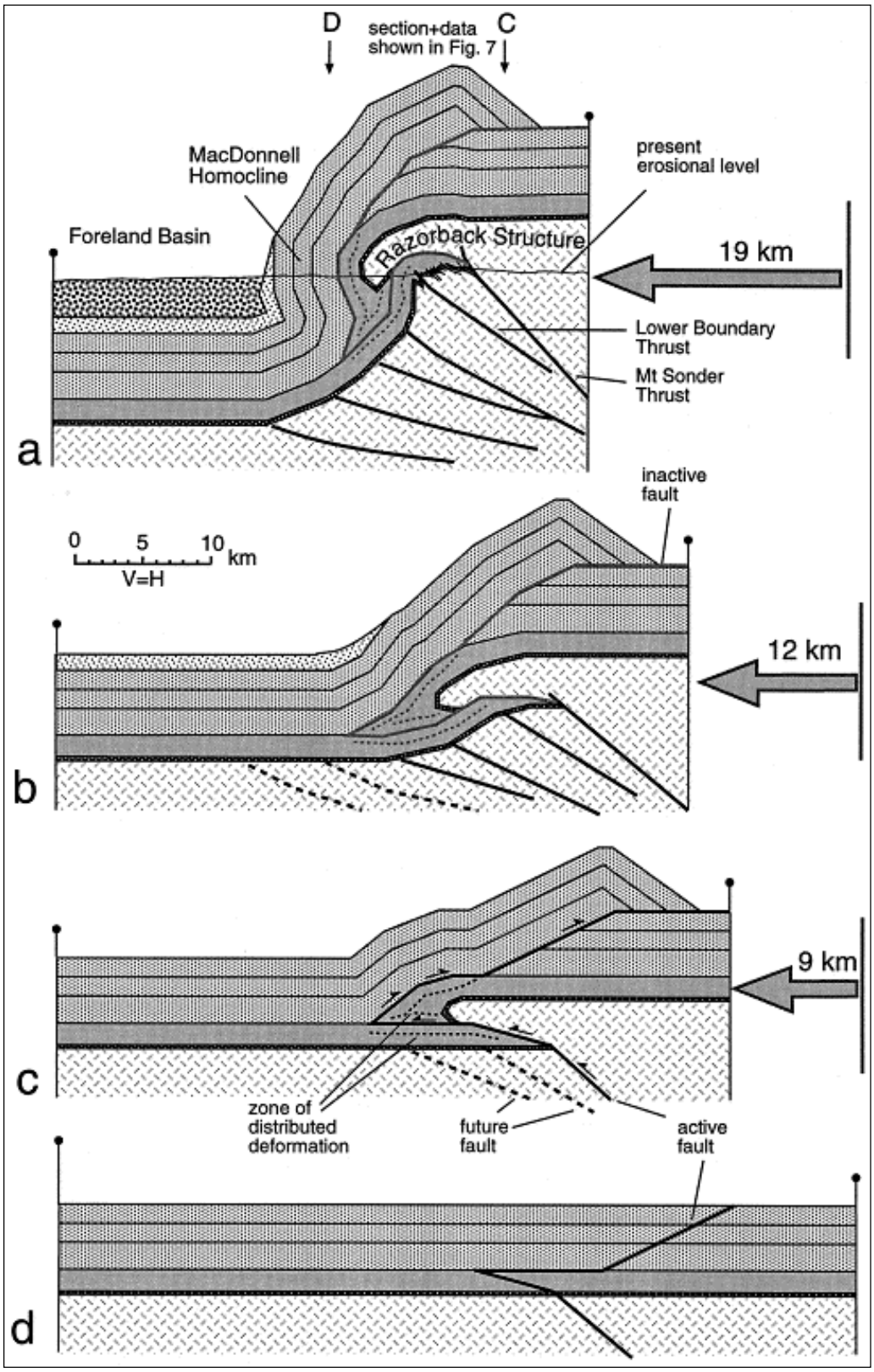

Figure 17

Ormiston Gorge section trace (Flottmann & Hand, 1999)

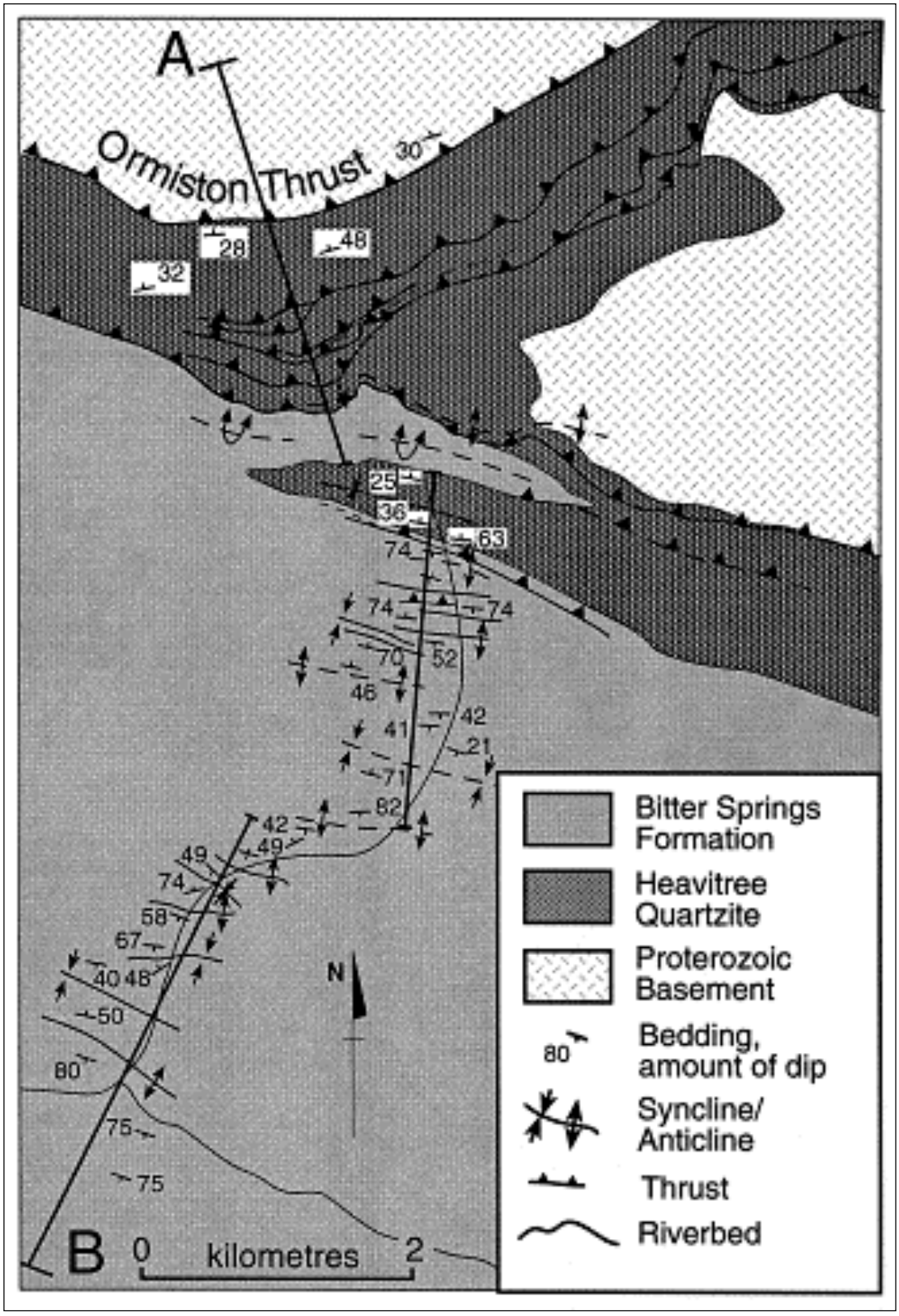

Figure 18

Ormiston Gorge cross-section – restored section (Flottmann & Hand, 1999)

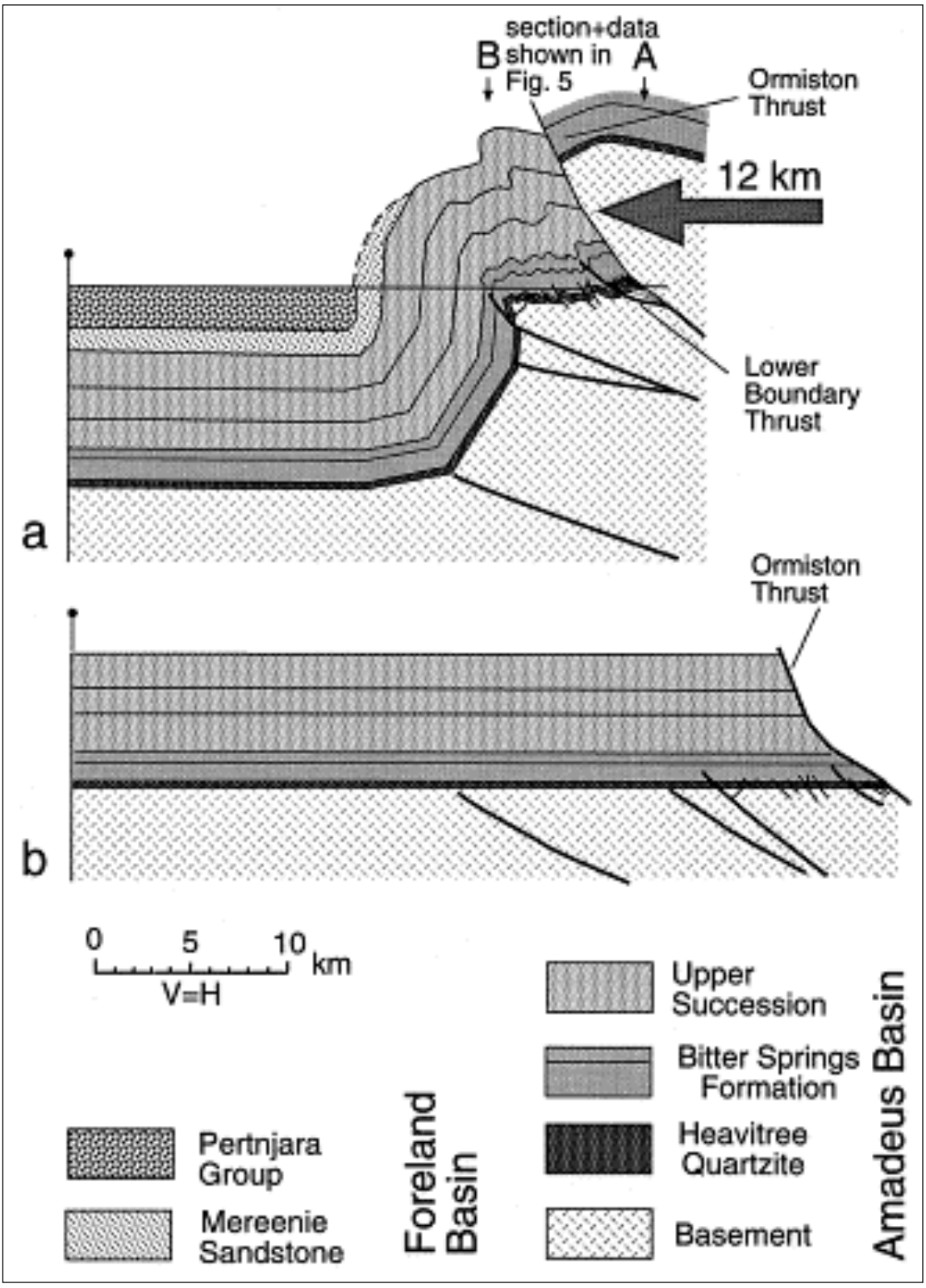

Figure 19

West of Ormiston Gorge

(266364 7393203)

(266364 7374840)

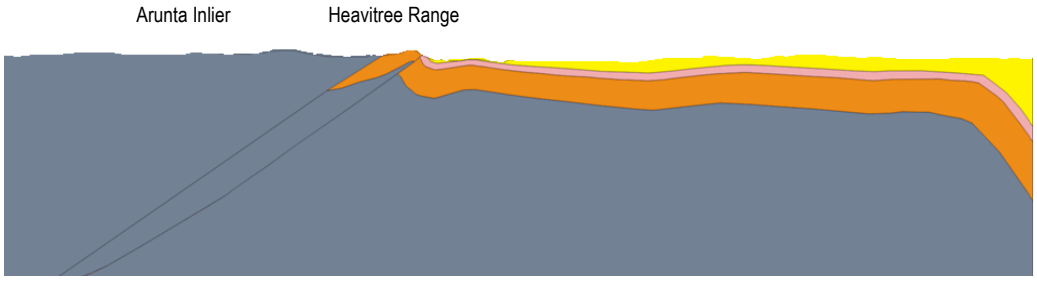

Geological cross-section: current-level

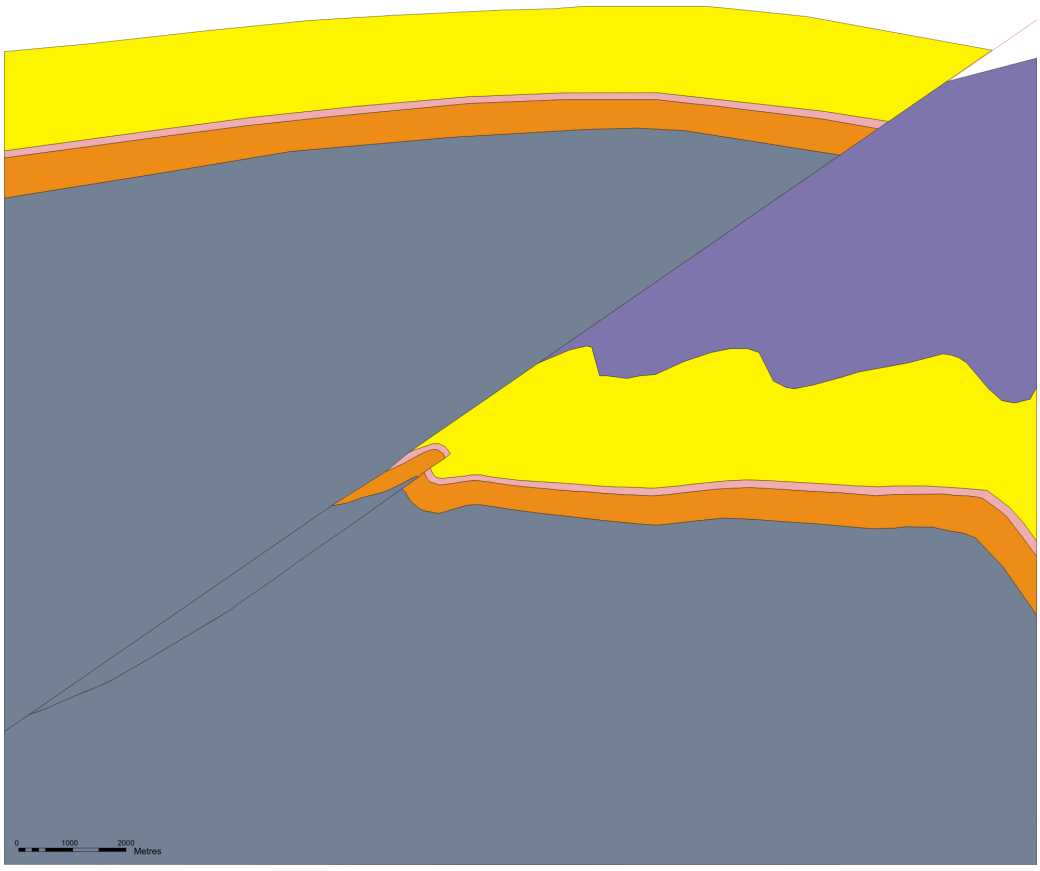

Reconstructed geological cross-section: pre-erosion

ID	Lithology
	Arunta Block
	Lower Heavitree Quartzite
	Upper Heavitree Quartzite
	Bitterspring Formation
	Upper Succession

Figure 20

Ormiston Gorge

(268 333 7389375)

(268 333 7372489)

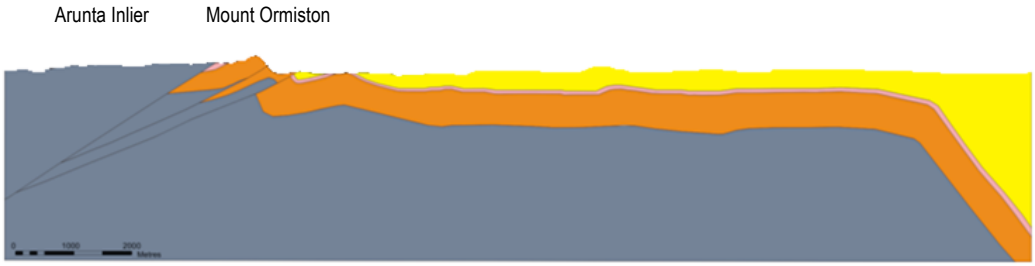

Geological cross-section: current-level

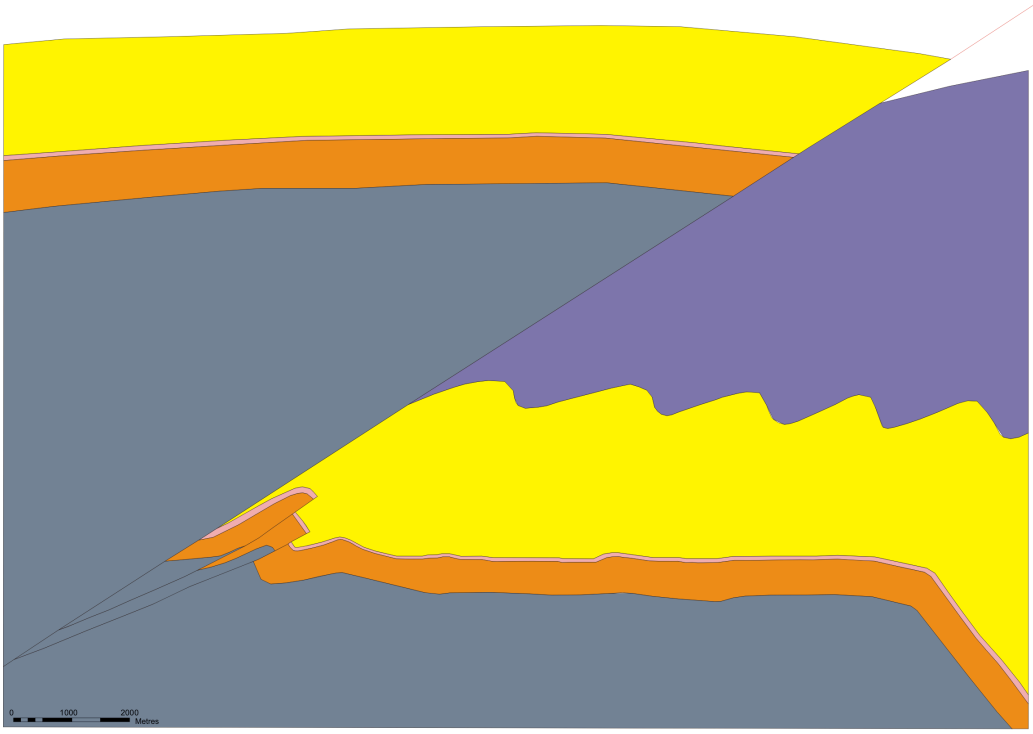

Reconstructed geological cross-section: pre-erosion

ID	Lithology
	Arunta Block
	Lower Heavitree Quartzite
	Upper Heavitree Quartzite
	Bittersprings Formation
	Upper Succession

Figure 21

Back Gorge

(268 480 7388248)

(271260 7384445)

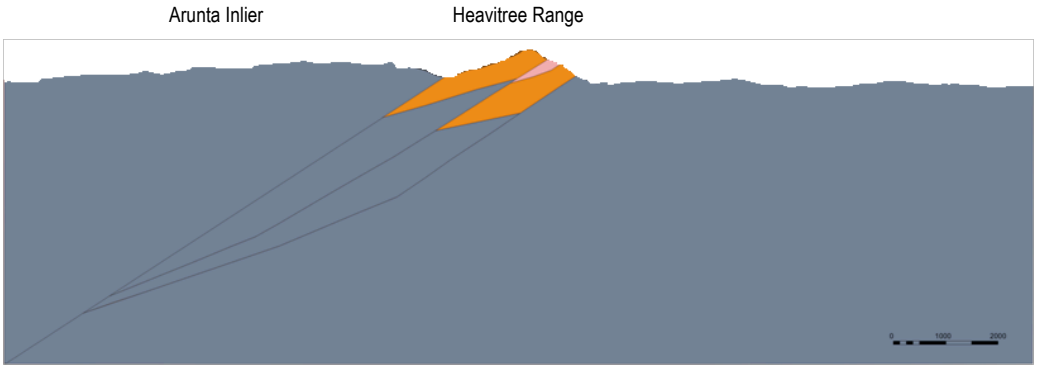

Geological cross-section: current-level

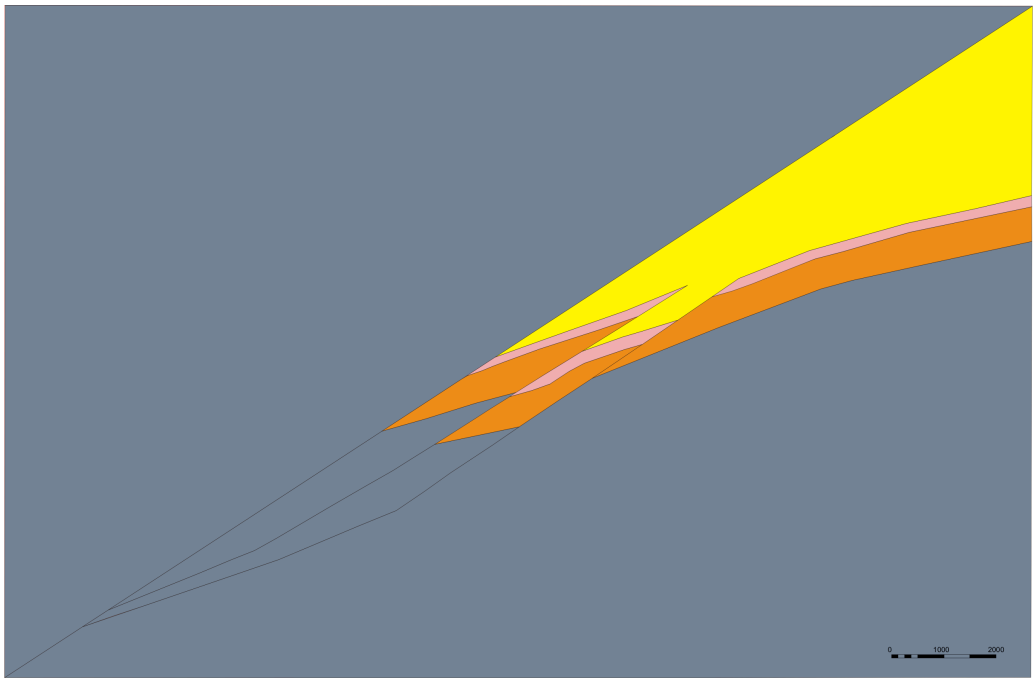

Reconstructed cross-section: pre-erosion

ID	Lithology
	Arunta Block
	Lower Heavitree Quartzite
	Upper Heavitree Quartzite
	Bittersprings Formation
	Upper Succession

Figure 22

Ormiston Pound

(274 276 7392200)

(274 234 7376202)

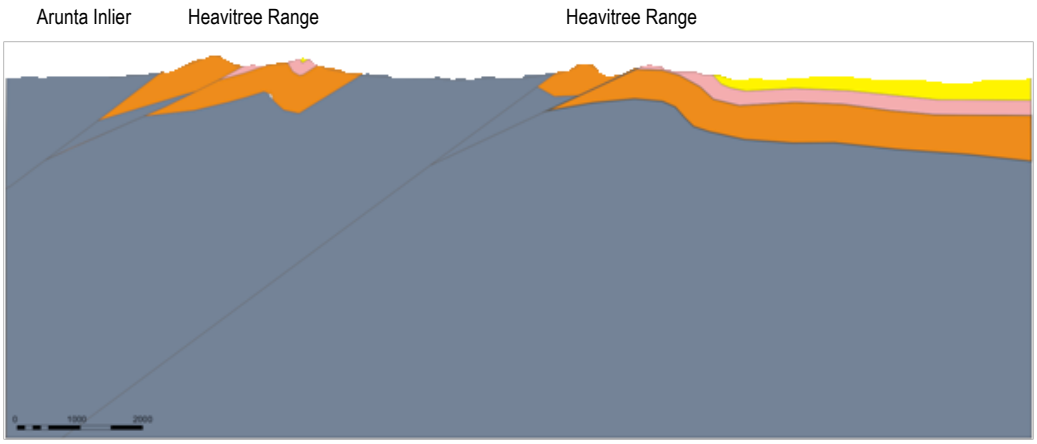

Geological cross-section: current-level

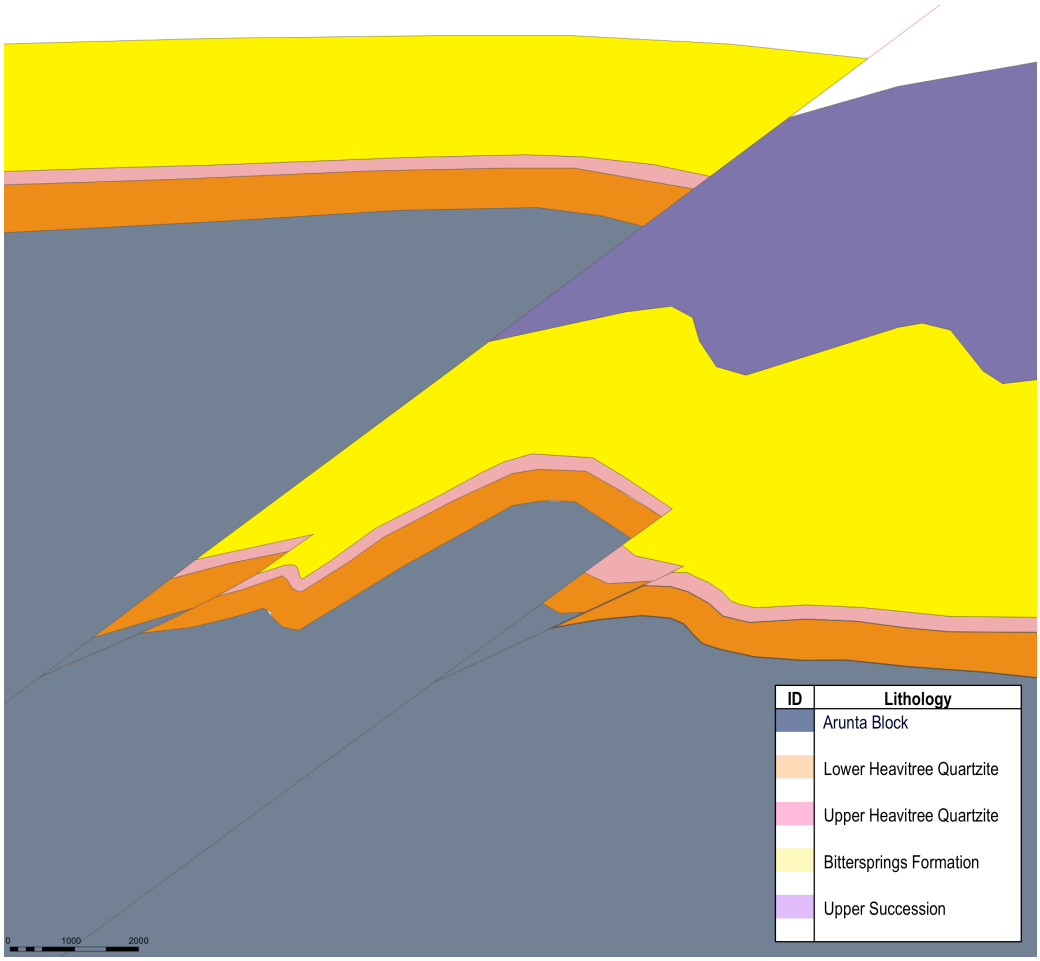

Reconstructed geological cross-section: pre-erosion

Figure 23